AD-A121 299 ANALYSIS OF IMBEDDED TRANSONIC SHOCK WAVE INFLUENCE ON TURBULENT BOUNDARY..(U) UNITED TECHNOLOGIES RESEARCH CENTER EAST HARTFORD CT J E CARTER ET AL. SEP 82 1/1

UNCLASSIFIED UTRC/R82-915712-1 AFOSR-TR-82-0955 F/G 20/4 NL

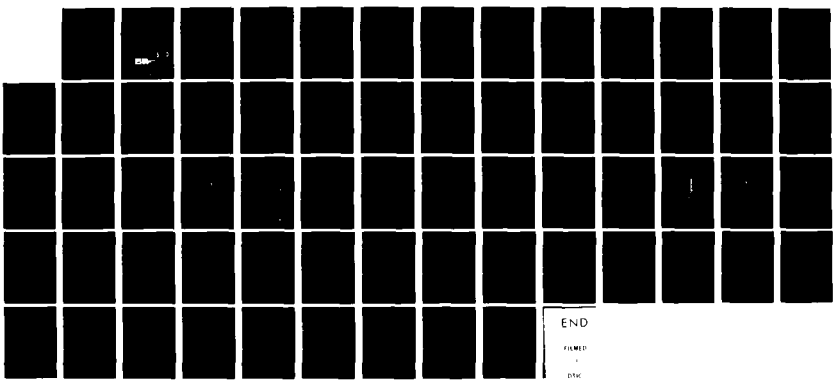

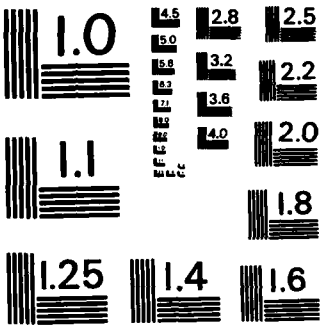

R82-915712-1

AFOSR-TR- 82-0955

(3)

ANALYSIS OF IMBEDDED TRANSONIC SHOCK WAVE INFLUENCE ON TURBULENT BOUNDARY LAYER SEPARATION

J.E. Carter and M.M. Hafez
September, 1982

Annual Report on Contract F49620-81-C-0041
for
Air Force Office of Scientific Research
Boiling Air Force Base, Building 410
Washington, D.C. 20332

UNITED TECHNOLOGIES RESEARCH CENTER
East Hartford, Connecticut 06108

UNCLASSIFIED

SECURITY CLASSIFICATION OF THIS PAGE (When Data Entered)

REPORT DOCUMENTATION PAGE	READ INSTRUCTIONS BEFORE COMPLETING FORM
1. REPORT NUMBER: AFOSR-TR- 82-0955	2. GOVT ACCESSION NO. AD-A121279 / 3. RECIPIENT'S CATALOG NUMBER
4. TITLE (and Subtitle): Analysis of Imbedded Transonic Shock Wave Influence on Turbulent Boundary Layer Separation	5. TYPE OF REPORT & PERIOD COVERED: Annual Report, 1 April 81 - 31 August 82
	6. PERFORMING ORG. REPORT NUMBER: R82-915712-1
7. AUTHOR(s): J. E. Carter, M. M. Hafez	8. CONTRACT OR GRANT NUMBER(s): F49620-81-C-0041
9. PERFORMING ORGANIZATION NAME AND ADDRESS: United Technologies Research Center, Silver Lane, East Hartford, CT 06108	10. PROGRAM ELEMENT, PROJECT, TASK AREA & WORK UNIT NUMBERS: 61102F, 2307/A1
11. CONTROLLING OFFICE NAME AND ADDRESS: AFOSR/NA, Bolling Air Force Base, Washington, DC 20332	12. REPORT DATE: September 1982
	13. NUMBER OF PAGES: 59
14. MONITORING AGENCY NAME & ADDRESS (if different from Controlling Office)	15. SECURITY CLASS. (of this report): Unclassified
	15a. DECLASSIFICATION/DOWNGRADING SCHEDULE

16. DISTRIBUTION STATEMENT (of this Report)

Approved for Public Release; Distribution Unlimited.

17. DISTRIBUTION STATEMENT (of the abstract entered in Block 20, if different from Report)

18. SUPPLEMENTARY NOTES

19. KEY WORDS (Continue on reverse side if necessary and identify by block number)

Transonic flow, shock boundary-layer interaction, separated flow, inverse boundary-layer

20. ABSTRACT (Continue on reverse side if necessary and identify by block number)

A strong viscous-inviscid interaction model has been developed for predicting the detailed properties of the flow in the vicinity of an imbedded transonic shock wave interacting with a turbulent boundary layer in cases where the shock wave is of sufficient strength to result in flow separation. In this interaction model the inviscid flow is analyzed with a compressible stream function analysis specifically developed for mixed subsonic-supersonic flow regions. In the present effort this analysis has been extended to include

DD FORM 1 JAN 73 1473 EDITION OF 1 NOV 65 IS OBSOLETE

S/N 0102-LF-014-6601

UNCLASSIFIED

SECURITY CLASSIFICATION OF THIS PAGE (When Data Entered)

upstream vorticity effects and the boundary-layer displacement effects. Numerous calculations are presented which demonstrate the capability of this analysis to predict transonic rotational flow. The viscous flow analysis in this interaction model is a newly developed inverse boundary-layer analysis which accounts for normal pressure gradients and imbedded shock waves. The equations are solved with a coupled implicit finite-difference scheme subject to the condition that the flow at the edge of viscous layer merges asymptotically with the outer inviscid flow. A model problem has been analyzed with this generalized inverse boundary-layer procedure and no stability problems were encountered. The first-order version of this inverse boundary-layer analysis has been applied to the transonic shock boundary-layer interaction studied by Kooi and comparison with this data is presented herein. In the future, work will be directed toward iteratively coupling these two analyses to provide an overall prediction method for transonic shock wave boundary-layer interaction.

R82-915712-1

Analysis of Imbedded Transonic Shock Wave Influence on Turbulent Boundary Layer Separation

TABLE OF CONTENTS

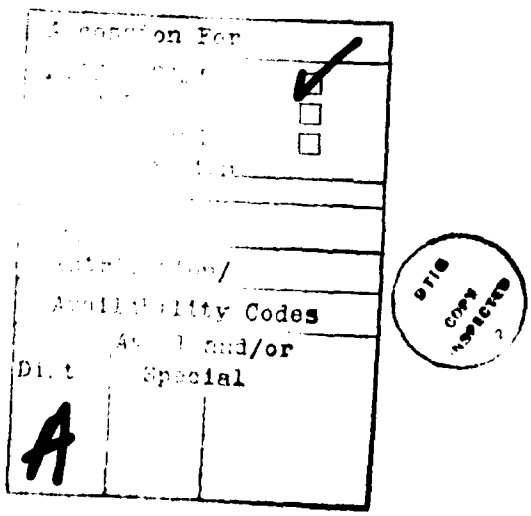

SUMMARY

The prediction of the flow field in transonic shock-wave boundary-layer interaction is an aerodynamic problem of immense practical importance in both external aerodynamics and turbomachinery applications since this flow phenomena has a large influence on the overall aerodynamic forces and often determines the upper limit in performance of each aerodynamic component. The main objective of the present research program is the development of an analytical/computational procedure for predicting the detailed properties of the flow in the vicinity of an imbedded transonic shock wave interacting with a turbulent boundary layer in cases where the shock wave is of sufficient strength to result in flow separation. This objective is being pursued through the development of a viscous-inviscid strong interaction model in which the inviscid flow is analyzed with a compressible stream function analysis including rotational flow effects, and the viscous flow is analyzed with a generalized inverse boundary-layer analysis which accounts for normal pressure gradients and imbedded shock waves. In the present program work on each of these analyses has been performed and the progress to date is reported herein.

The compressible stream function analysis of Hafez has been extended to flows with upstream vorticity and calculations have been made both for subsonic nonuniform flow over a thin airfoil and transonic shock-wave boundary-layer interaction. Comparisons are presented of these results with the previous Euler calculations of Steger and Lomax for the airfoil flow and the asymptotic analysis of Melnik and Grossman for a normal shock impinging on a turbulent boundary layer. Overall the agreement obtained between the present inviscid analysis and these previous results is good thereby verifying the present formulation and numerical procedure for the solution of the compressible stream function equation including vorticity. In addition preliminary results have been obtained with this inviscid method for the transonic shock boundary layer interaction studied experimentally by Kooi. These results indicate that for cases in which the shock wave is of sufficient strength to separate boundary layer, inclusion of both the boundary layer displacement thickness and upstream vorticity have a significant effect on the computed inviscid flow field.

Guided by the detailed experimental measurements and conclusions made by Kooi for separated transonic shock-wave boundary-layer interaction, a viscous formulation has been established which includes the variation of the pressure across the boundary layer. In this flow model, it is assumed that the y-variation of the streamwise pressure gradient is that deduced in the rotational inviscid analysis over the displacement body, the definition of which has been suitably generalized to account for the variation of the inviscid flow on the scale of the boundary-layer thickness. In this viscous formulation, the

governing equations and boundary conditions have been derived in such a manner that the boundary-layer solution blends smoothly into the inviscid solution as the edge of the viscous layer is approached. This viscous formulation is a generalization of the first-order inverse boundary-layer analysis previously developed by Carter for the analysis of separated turbulent flows. Results are presented for a model problem of incompressible separated flow which demonstrates that the present formulation is stable and is capable of solving separated turbulent flows with significant variation in the pressure across the boundary layer. In addition preliminary viscous flow results have been obtained for the Kooi transonic case by solving the first-order inverse boundary-layer equations for a prescribed displacement thickness which was measured experimentally by Kooi. The computed results are in qualitative agreement with the data, but they indicate a larger separation bubble than that measured by Kooi. Further work is needed to determine whether this difference is due to higher order boundary-layer effects or turbulence modeling or both.

INTRODUCTION

The intersection of a shock wave with a turbulent boundary layer in transonic flow results in a complex flow pattern for which a reliable and accurate prediction method has yet to be developed. The problem is complicated by the fact that the shock is generally thought to penetrate the boundary layer thereby inducing discontinuities in the boundary-layer flow variables in addition to the large streamwise changes which occur as the turbulent boundary layer responds to a large pressure increase. As the shock strength is increased flow separation occurs; this in turn displaces the outer inviscid flow, and consequently the shock location and detailed flow field in the vicinity of the shock are significantly different from that predicted by inviscid flow. The determination of the reattachment location (if it occurs at all) and thus the extent of the separated region is also an important part of an aerodynamic analysis of transonic flows containing shock waves.

Transonic shock wave boundary-layer interaction is an aerodynamic problem of immense practical importance because of the frequent occurrence of this phenomena in many types of configurations. Examples include airfoils in supercritical flow - both external and internal (turbomachinery applications), exhaust nozzles, and engine inlets. These interactions can lead to premature separation which can result in buffeting, large decreases in drag, and reduced engine performance. In addition, it is difficult to predict full scale shock interaction phenomena from smaller scale wind tunnel data because of the current inability to match experimentally full scale Reynolds number flows. Hence, there is a strong need to develop analytical and computational techniques for the analysis of the problem of transonic shock wave boundary-layer interaction.

The overall goal of this research program is the development of a reliable and accurate method for predicting the detailed properties of the flow in the vicinity of an imbedded transonic shock interacting with a turbulent boundary layer. This goal is being pursued through the development of a viscous-inviscid interaction model suitably generalized to account for rotational flow effects in the inviscid flow analysis and normal pressure gradients and imbedded shock waves in the viscous analysis. In the past year work has been performed on the individual inviscid and viscous components of this interaction analysis and these developments are reported herein. In the next phase of this work a technique will be developed for coupling these analyses together for the iterative calculation of the viscous and inviscid governing equations for the solution of transonic shock-wave boundary-layer interaction where the shock wave is of sufficient strength to result in flow separation.

BACKGROUND

A number of different approaches have been pursued in attempts to develop a reliable and accurate prediction method for transonic and shock-wave boundary-layer interaction. There have been numerous attempts (e.g., see Refs. 1-2) to solve numerically the Navier-Stokes equations for this flow field; but to date the comparisons of these solutions with experimental data have not been particularly good. This lack of agreement is probably due to the current lack of an adequate turbulence model for this type of strongly interacting flow and the inability of most grid distributions used in the numerical solutions of the Navier-Stokes equations to resolve adequately the fine details of the flow. It is unlikely that this type of brute force approach on such a multiple scale problem will yield a practical engineering method in the near future; nonetheless, this approach can serve to provide benchmark solutions to evaluate more expedient, but approximate techniques. An earlier example of this type of evaluation is the comparison between the Navier-Stokes solutions of Carter (Ref. 3) and the interacting boundary-layer solutions of Werle and Vatsa (Ref. 4) for supersonic laminar separated flow. A more recent example of this type of comparison is presented in Ref. 5 in which the Navier-Stokes calculations of Swanson are compared with the interacting boundary-layer solutions of Vatsa and Carter for the subsonic turbulent separated flow over a boattail-sting configuration.

A number of approximate techniques have been developed for the analysis of transonic shock-wave boundary-layer interaction. These methods include both the classical boundary layer/inviscid matching procedure due to Prandtl and the more recent inverse boundary-layer/inviscid matching procedure. In the classical approach, as exemplified by the approaches of Garabedian, Korn, and Bauer (Ref. 6) and Carlson (Ref. 7), the boundary-layer solution is obtained in a conventional manner by imposing the pressure distribution deduced from the inviscid solution. It is well known that a direct solution (pressure prescribed) of the boundary-layer equations is singular at separation, provided the boundary-layer solution is accurately obtained. In Refs. 6 and 7 this separation singularity does not occur because the approximate boundary-layer solution obtained from the integral form of the boundary-layer equations is not sufficiently accurate. In fact, it is difficult to estimate the point of separation in these approaches and thus an empirical criterion is used to estimate separation; reattachment is determined from an ad hoc shape factor criterion.

The separation singularity in the boundary-layer equations can be eliminated by solving the equations inversely; that is, instead of prescribing the pressure

as is done in the direct approach, another quantity such as the displacement thickness (Ref. 8 and 9) or skin friction (Refs. 9 and 10) is prescribed. The pressure distribution is computed from the resulting boundary-layer solution. Since the solution at separation is regular it can be continued downstream into the separated region and through the point of reattachment. The inverse boundary-layer approach has been improved significantly since the earlier works cited above, and in fact, has now been developed (see Ref. 11) to the point where compressible turbulent separated flows can be routinely calculated. The next step in the use of the inverse boundary-layer theory is that it has to be iteratively combined with an inviscid calculation so that the displacement thickness interaction of the viscous and inviscid flow can be computed. Several techniques have been developed, but the recent viscous/inviscid interaction technique developed by Carter (Ref. 12) is beginning to receive wide use (Refs. 13-16) due to its simplicity and rapid convergence. A similar procedure has been developed by LeBalleur (Ref. 17) which he used to couple an inviscid analysis with an inverse integral boundary-layer method for the computation of transonic flow over a lifting airfoil. Recently Wigton (Ref. 18) has performed a von Neumann stability analysis of both the LeBalleur and Carter coupling procedures for both subsonic and supersonic flows.

At the present time, the Carter iterative technique, in which the inverse finite-difference boundary-layer method of Ref. 11 is coupled to a transonic relaxation solution of the full potential equation is being applied to a transonic flow problem with the support of the Office of Naval Research (Ref. 19). The purpose of this contract is to determine if this interaction procedure, previously demonstrated for subsonic flows, can be applied to flows with shock waves. Despite the approximate nature of these calculations, which is due to the neglect of imbedded shock effects, the results of this investigation should provide information which will facilitate the detailed transonic analysis discussed herein. Typical results which have been obtained thus far in this contract, using both the nonconservative (NC) potential flow analysis of South and Jameson (Ref. 20) and the fully conservative (FC) potential flow analysis of Green (Ref. 21), are shown in Fig. 1 in which comparisons are made with experimental data and the Navier-Stokes results obtained at NASA-Ames (Ref. 2) for the case of shock induced separated flow over an axisymmetric body.

Interaction techniques based on an inverse boundary-layer approach are certainly an improvement over direct procedures since the separated flow can be computed free of singularities. Nonetheless, the fundamental flow model used in the above-mentioned interaction procedures assumes that the shock wave does not penetrate the boundary layer and furthermore that normal pressure gradients are negligible. This type of model is applicable to laminar supersonic flows in which shock boundary-layer interaction occurs; it has successfully been used by many investigators such as Werle and Vatsa (Ref. 4) in their analysis of the

interacting boundary-layer equations. In the turbulent case the flow model is quite different from that in laminar flow as discussed by Melnik (Ref. 22) and others. One important difference is that in the turbulent case the streamwise length scale of the interaction is quite small (less than 10 upstream boundary-layer thicknesses) thereby resulting in significant flow turning and normal pressure gradients as the turbulent boundary layer responds to the shock wave. Most of this flow turning occurs in the outer part of the turbulent boundary layer which, as first observed by Lighthill (Ref. 23) acts essentially as an inviscid rotational layer. In the transonic case, the interaction of a normal shock wave with a turbulent boundary layer results in two distinct flow patterns depending on whether the shock is of sufficient strength to separate the boundary layer. These flow patterns are shown schematically in Fig. 2. In the case of attached flow, a single shock appears whereas if the flow is separated, a lamda shock results. It is not known if the appearance of the lamda shock occurs simultaneously with the occurrence of the flow separation; however, these two phenomena are generally associated with each other. Another important issue in the turbulent shock boundary-layer interaction problem is whether or not the shock wave penetrates the boundary layer, that is, do the compression waves which result when the shock strikes the rotational flow coalesce inside or outside of the viscous layer? The location of the shock formation depends essentially on the oncoming Mach number which in turn determines the sonic line location. For Mach numbers near one, where the shock is weak, the sonic line lies near the boundary-layer edge. As the Mach number is increased, the sonic line moves closer to the surface and thus focusing of the compression waves, which eminate from the sonic line occurs lower in the boundary layer. In the experimental studies of Kooi (Ref. 24) on transonic shock wave boundary-layer interaction, it was observed that at a free stream Mach number of 1.40 compression wave coalescence occurs well outside the boundary layer to form the forward leg of the oblique shock. At a higher Mach number of 1.54 East (Ref. 25) observed that "the oblique shock was formed at the edge or probably even inside the boundary layer". Clearly, the development of a theoretical method which allows for imbedded shock effects would increase the current ability to quantitatively predict the influence of Mach and Reynolds number on transonic interactions.

In recent years, asymptotic methods of analysis have been used by Melnik and Grossman (Ref. 26), Adamson and Feo (Ref. 27), and by Messiter (Ref. 28) for normal and oblique shock waves impinging on a turbulent boundary layer over a flat plate in transonic flow. At the present time, only the attached flow case has been treated. The use of asymptotic theory has delineated the mathematical structure of the flow field and has shown that, in the absence of flow separation, the outer layer, comprised of the external flow and the main part of the boundary layer which is represented as an inviscid rotational flow, is unaffected by flow changes in the thin viscous sublayer near the wall. This flow behavior

points out the large difference between laminar and turbulent interactions since in the laminar case the main part of the boundary layer is affected by the growth of the viscous sublayer no matter how weak the shock wave may be. For the turbulent attached flow case, Melnik and Grossman (Ref. 1) numerically obtained solutions to the inviscid nonlinear governing equations which resulted from their asymptotic analysis. Their solutions demonstrate that the mechanism which causes the shock to bend forward and blend smoothly into the sonic line is contained entirely in the interaction between the inviscid rotational flow and externally imposed shock wave. Their analysis applies to the weak viscous interaction case shown in Fig. 2; the objective of the present program, which is described in the remainder of this annual report, is the development of a procedure for analyzing the strong interaction case also shown in Fig. 2.

VISCOUS-INVISCID INTERACTION FLOW MODEL

For the strong interaction flow problem shown in Fig. 2, a flow model has not as yet been developed from asymptotic theory. Instead, we are currently developing an analytical model, shown schematically in Fig. 3, which is basically an extension of that developed from asymptotic theory for weak interactions but modified as needed for the more severe case when flow separation occurs. This model has similar concepts to that recently proposed by LeBalleur, et al. (Ref. 29) and East (Ref. 30). In this model, as in the weak interaction case, the outer part of the turbulent boundary layer is treated as an inviscid rotational flow where the rotationality is due both to the upstream boundary layer as well as to the curved shock waves. This inviscid rotational flow is analyzed using the recently developed compressible stream function approach of Hafez (Ref. 31). In contrast to the potential approach, the stream function analysis is applicable to flows in which the vorticity is non-zero. In the weak interaction case the viscous layer is passive and does not have to be considered to determine the surface pressure; in the strong interaction case the viscous layer is active and is represented by a generalized displacement surface. The displacement surface is deduced as usual by asymptotic matching of the viscous and inviscid flows, suitably generalized to account for the variation of the inviscid rotational flow in the outer part of the viscous region. Figure 4 shows the matching of the viscous and inviscid velocity profiles as the edge of the viscous layer is approached.

The viscous-layer analysis in this flow model extends from the wall to the edge of the viscous region as shown in Fig. 3, but differs from a conventional boundary-layer analysis in that normal pressure gradients and imbedded shock effects are included by a generalization of the inverse boundary-layer procedure of Carter (Ref. 32) which was specifically developed for the analysis of separated flows. This flow model results in a large overlap region between the viscous and inviscid region in the outer part of the boundary layer; to align these analyses the viscous equations are solved subject to the imposed lateral pressure variation deduced in the inviscid calculation. An alternative formulation which will be developed in next year's program is to solve the viscous-layer equations only from the wall to the inner part of the outer inviscid rotational-layer. This approach probably avoids the issue of including normal pressure gradients in the viscous layer analysis but now a difficult matching problem is encountered in matching the viscous and inviscid solutions in the interior of the boundary layer where the shear is non-zero.

INVISCID ANALYSIS

The compressible stream function analysis of Ha_.z (Ref. 31) had previously been applied to problems in which the freestream flow was irrotational. For rotational flows, the stream function equation is written as

$$\frac{\partial}{\partial x}\left(\frac{1}{\rho}\frac{\partial \psi}{\partial x}\right)+\frac{\partial}{\partial y}\left(\frac{1}{\rho}\frac{\partial \psi}{\partial y}\right)=-\omega \tag{1}$$

where the vorticity can be rewritten, using Crocco's relation, in terms of the entropy S and the total enthalpy H, as

$$\omega = p\frac{dS/R}{d\psi} - \rho\frac{dH}{d\psi} \tag{2}$$

Equations (1) and (2) can be solved iteratively where the vorticity is evaluated from the previous iterations with the pressure given by

$$p = \frac{\rho^{\gamma}}{\gamma M_{\infty}^2} e^{S/c_v} \tag{3}$$

and the density deduced from

$$\rho = \left[(\gamma-1)\ M_{\infty}^2 H - \frac{\gamma-1}{2} M_{\infty}^2\left(u^2+v^2\right)\right]^{\frac{1}{\gamma-1}} e^{-S/R} \tag{4}$$

This formulation is equivalent to that given by the Euler equations which are based on the conservation laws for mass, momentum and energy.

As a test of the above stream function formulation, calculations were performed for the accelerated and heated subsonic flow over a 6 percent thick parabolic arc airfoil, previously analyzed by Steger and Lomax (Ref. 33) with the Euler equations. In this initial test the analysis was simplified by assuming that the entropy and total enthalpy and hence, the vorticity were a function of the distance y normal to the airfoil line of symmetry. Hence, the streamlines along which the upstream vorticity is convected are assumed to be parallel.

The computed pressure distributions on the airfoil for $M_{\infty} = .4$ are shown in Fig. 5 in comparison with the solutions of the Euler equations deduced by Steger and Lomax (Ref. 33). For the irrotational case ($\delta = 0$) excellent agreement is observed for the airfoil pressure distribution. As the magnitude of

the nonuniformity of the freestream is increased the two results diverge slightly apparently due to the parallel flow approximation in the present analysis. This limitation can be straightforwardly relieved by using a one-dimensional spline fit of the entropy and total enthalpy as a function of the stream function in order to account for the precise dependence of the voriticity on the streamline location.

Figure 6 shows the convergence history for the present calculation in which a variable grid of 60 by 40 grid points were distributed over a computational region which extended about 3 chords in the x-direction and 3.5 chords in the y-direction. Figure 6 shows that R_{max}, the maximum residual in the finite-difference equations between two successive iterations, decreases rapidly with the present numerical scheme and, suprisingly, the convergence is more rapid with the inclusion of finite vorticity in the governing equations.

A second problem which has been analyzed in the present effort is the interaction of a normal shock wave with the outer inviscid rotational part of a turbulent boundary layer. The particular problem chosen is the weak interaction case analyzed by Melnik and Grossman (Ref. 26) which was discussed earlier and is shown schematically in Fig. 2. Melnik and Grossman obtained numerical solutions to the asymptotic equations which they derived in the double limit of Reynolds number approaching infinity and free stream Mach number approaching unity. They expressed this double limit in terms of a similarity parameter, χ_t, defined by

$$\chi_t \equiv \frac{M_\infty^2-1}{\epsilon} \tag{5}$$

where $\epsilon = \sqrt{c_{f_o}/2}$, which is the nondimensional friction velocity of the approaching boundary layer. In the limit of infinite Reynolds number, ϵ approaches zero. The asymptotic formulation which was derived by Melnik and Grossman has explicit dependence only on the similarity parameter χ_t, not the individual Mach and Reynolds numbers.

In order to make a comparison of the numerical results from the present formulation with the asymptotic results of Melnik and Grossman, it was necessary to assume a value of the free stream Mach number. Since the Melnik-Grossman theory is limited to the weak interaction (non-separated) regime for which the Mach number is limited to 1.2 and smaller, values of $M_\infty = 1.12$, 1.08 and 1.04 were chosen for the present comparison. Melnik and Grossman presented calculations for $\chi_t = 7.5$ which results in $\epsilon = .034$, .022 and .011 for the three respective Mach numbers. The incoming velocity profile was specified in

the same manner as Melnik and Grossman by prescribing

$$u = 1 + \varepsilon\, u_i(y) \tag{6}$$

where $u_i(y)$ is Coles' (Ref. 34) wall-wake representation of a turbulent boundary layer.

Figure 7 shows a comparison of the wall pressure distributions obtained from the present analysis with that computed by Melnik and Grossman. It is seen from both calculations that the interaction of the incident normal shock, which is located at X = 0, with the incoming rotational flow results in a continuous but steep pressure rise at the wall, as is observed experimentally. The short streamwise length scale of this interaction is evident from Fig. 7 since most of the pressure rise occurs in about 8 incoming boundary layer thicknesses (δ_o). It is observed in Fig. 7 that the pressure distributions computed from the present analysis are well correlated by the similarity variables established by the asymptotic analysis of Melnik and Grossman. While the agreement between the present solutions and that of Melnik and Grossman can be considered encouraging in an overall sense, it is not clear why differences remain. The most obvious candidate for explaining the differences is that no attempt was made in this comparison to insure that the mesh sizes were the same. Hence, further calculations are needed in which the mesh size is reduced in the present analysis with this mesh reduction guided by the asymptotic analysis of Melnik and Grossman.

Figure 8 shows the convergence history of the present numerical procedure for this transonic case where $M_\infty = 1.2$. In the supersonic region, a retarded density technique which was developed by Hafez, South and Murman (Ref. 35), was used to introduce artificial viscosity which is necessary for convergence. The retarded density is given by

$$\tilde{\rho} = \rho - u\,\frac{\partial \rho}{\partial x}\,\Delta x \tag{7}$$

where μ is a switch factor given by

$$\mu = \max\left(0,\ 1 - \frac{1}{M^2}\right) \tag{8}$$

where M is the local Mach number. Calculations were also made with a constant value of μ independent of whether the flow is subsonic. It is observed in Fig. 8 that the use of a constant value of artificial viscosity coefficient results in a more rapid convergence rate than that found with a variable viscosity coefficient. This increase in the convergence rate is probably due to the smoother solution which is obtained for $\mu = .6$. The constant viscosity model is very similar to the analysis of the viscous transonic equation made by Sichel for transonic shock bifurcation.

The numerical results presented herein were obtained using the explicit marching procedure of Hafez and Lovell (Ref. 31) to update the u-component of velocity after each relaxation cycle. In the present calculations it was found that the convergence was enhanced by using mixed flow differencing techniques in this marching procedure. However, this method is still sensitive to the mesh size in the y-direction and hence should be replaced by an unconditionally stable implicit conservation procedure. The implicit scheme suggested here is to re-write Eq. (1) in terms of the speed q, namely,

$$-\frac{\partial}{\partial x}\ (q \sin\theta) + \frac{\partial}{\partial y}\ (q \cos\theta) = -\omega \tag{9}$$

where,

$$\tan\theta = \frac{v}{u} = -\frac{\frac{\partial\psi}{\partial x}}{\frac{\partial\psi}{\partial y}} \tag{10}$$

Equation (9) is treated as a single equation in q assuming θ is known from the previous iteration. Using proper upwind differencing of both x- and y-terms leads to a stable calculation. Once q is known the density is calculated based on Eq. (4). This scheme has been implemented with almost the same computational rate as the explicit scheme previously used in Ref. 31.

Finally, in order to test the present inviscid analysis for stronger shock waves, a model problem similar to Kooi's experiment (Ref. 24) was tested numerically. In this experiment a normal shock impinges on a turbulent boundary layer which results in a separation bubble shown in Fig. 9, which was reproduced from Kooi's report (Ref. 24). For this case $M_\infty = 1.4$ and the Reynolds number, based on the momentum thickness at the start of the interaction, is 2×10^4. The characteristics of the undisturbed boundary layer just upstream of the interaction region are:

$$\delta_o = 6.6 \text{ mm};\ \delta^* = 1.06 \text{ mm},\ \theta = .49 \text{ mm},\ c_f = .0019$$

The velocity profile utilized in this calculation is the same as that used previously, Eq. (6), with $\varepsilon = .031$ for this case. Good agreement was found between this wall-wake profile and the experimental data of Kooi as well as a solution of the direct form of the present boundary-layer analysis to be discussed in the next section. A uniform grid of 80 streamwise points and 40 transverse points was used with $\Delta x/\delta_o = 0.3$ and $\Delta y/\delta_o = 0.166$ in the calculation. Convergence was obtained using successive overrelaxation in about 500 iterations when the maximum residual decreased to 10^{-5}.

Figures 10 and 11 show the computed Mach contours for this case; in Fig. 10 the viscous displacement thickness has been ignored whereas in Fig. 11 a smooth approximation to the displacement thickness measured experimentally by Kooi has been included. Comparison of the Mach contours for these two calculations shows that the effect of the shock wave propagates further upstream when the viscous displacement effect is included and produces a resulting flow field picture which is in more qualitative agreement with that measured by Kooi than when the displacement thickness is ignored. Additional calculations showed that for higher Mach numbers the effects of δ^* is even more pronounced. In all of these calculations the pressure distribution at different y-levels was observed to become increasingly steeper with increased distance from the surface which is in qualitative agreement with the experimental measurements of Kooi (Ref. 24).

In these calculations the vorticity generated by the shock waves has not been accounted for and thus there is no shear layer in these results as there was in the experiment of Kooi due to shock bifurcation. Furthermore, in the present calculation the vorticity has been assumed to be a function of y only, i.e., $\omega = \omega(y)$, instead of $\omega/\rho = \omega/\rho\ (\psi)$. These assumptions can be overcome in the stream function formulation using a shock detection procedure and a spline fit for the vorticity as a function of the stream function. However, it appears that this procedure will be quite tedious and hence a new conservation method which eliminates the need for shock detection (or shock fitting), and vorticity tracking along streamlines is currently under development.

VISCOUS ANALYSIS

The viscous analysis currently under development in the present program is a generalization of the previous inverse boundary-layer method of Carter (Ref. 32) for the inclusion of normal pressure gradients and imbedded shock effects. In this new formulation the streamwise pressure gradient $\partial p/\partial x$, is now considered to be a function of both x and y. In this section a brief description of this approach will be given and results obtained for a model problem with separated flow and normal pressure gradients will be discussed.

In the present strong interaction flow model, shown schematically in Fig. 2, it is assumed that the inviscid flow is displaced outward due to the rapid boundary-layer growth which occurs downstream of the shock wave. However, the present problem is more complicated than conventional displacement thickness interaction since the usual assumption that the inviscid flow over the displacement body is invariant on the scale of the boundary-layer thickness is no longer applicable. As a result the usual definition of the displacement thickness must be generalized to account for this variation which leads to the defintion,

$$\int_0^\infty \rho u dy = \int_{\delta^*}^\infty \rho_i u_i dy \tag{11}$$

where the left integral is for the viscous flow and the right integral in which ρ_i and u_i are both dependent on y, is for the inviscid flow over the displacement body. Equation (11) insures that the mass flow is conserved between the viscous and the displacement induced inviscid flow.

Using this generalized definition of the displacement thickness, Kooi (Ref. 24) deduced several important conclusions from his experimental data for transonic shock-wave boundary-layer interaction which have been utilized in the development of the present formulation. First, he observed that the measured initial pressure rise over the displacement body agreed very well with that computed from simple wave theory in the supersonic portion of the flow which strongly supports the use of the displacement body concept for this flow. Second, he observed good agreement between his measured normal pressure gradients and that computed from simple wave theory for the inviscid flow over the generalized displacement body. As a result of this observation the streamwise pressure gradient, $\partial p/\partial x$ in the boundary-layer momentum equation

$$\rho u \frac{\partial u}{\partial x} + \rho v \frac{\partial u}{\partial y} = - \frac{\partial p}{\partial x} + \frac{\partial}{\partial y}\left(\mu_t \frac{\partial u}{\partial y}\right) \tag{12}$$

is assumed in the present formulation to be that of the rotational inviscid flow over the generalized displacement body. For the transonic problem under study this pressure gradient, which depends on both x and y, will be determined from the compressible stream function approach discussed earlier thereby accounting for the flow turning and hence normal pressure gradients and imbedded shock effects in the boundary layer.

In order to facilitate the numerical solution, the x-momentum, continuity, and energy equations are written in displacement body coordinates in which a modified form of the Levy-Lees transformation is used to transform these governing equations. At the present time the curvature of the displacement body has been neglected; however, this effect can be included later in a relatively straightforward manner. Based on previous work for separated boundary layers, it was decided to recast the governing equations and boundary conditions into an inverse formulation in which the pressure on the displacement body is deduced from the solution of the viscous equations for a prescribed streamwise distribution of boundary-layer perturbation mass flow

$$m = \rho_\delta^* u_\delta^* \delta^* \tag{13}$$

where ρ_δ^* and u_δ^* denote the inviscid density and tangential velocity over the displacement body and δ^* is the generalized displacement thickness defined in Eq. (11). At the wall the usual boundary conditions are imposed; at the outer edge of the boundary layer the viscous solution is required to merge smoothly into the inviscid solution as shown in Fig. 4 and thus the following conditions are imposed at each x-location.

$$u \to u_i(y), \quad \psi \to \psi_i(y) \tag{14}$$

where the subscript i denotes the inviscid solution. Note that the condition on the stream function, which is used instead of the v-component of velocity, automatically guarantees that the mass flow condition given in Eq. (11) is satisfied. In addition the $\partial p/\partial x$ term, which is assumed to be known from the inviscid solution, was rewritten in terms of the inviscid convection terms normalized with respect to the flow along the displacement body in the same manner as the boundary-layer convection terms. This last step is of critical importance since

it guarantees that the outer boundary conditions are asymptotic and can be imposed at any y-location provided the viscous stress terms are negligible which occurs as the boundary-layer edge is approached. The transformed governing equations and boundary conditions for the generalized inverse boundary-layer formulation were recently presented as part of a paper by Carter and Vatsa (Ref. 36). This paper is included in this Annual Report as Appendix A.

In order to test the convergence properties of the numerical scheme for this new formulation, a model problem for low speed separated flow was analyzed. The perturbation mass flow, m, which was prescribed for this model problem, is shown in Fig. 12 to depart rapidly from a flat plate turbulent flow distribution at X/L = 0.4 which is characteristic of the sudden boundary-layer growth which occurs when a normal shock wave impinges on a turbulent boundary-layer. Downstream of this rapid increase the displacement thickness typically reaches a maximum value and then decreases as the downstream adverse pressure gradient becomes smaller. The inviscid y-variation of the streamwise pressure gradient was imposed in the present formulation by assuming a linear variation of the inviscid velocity, $u_i(x,y)$ across the boundary layer. The slope of this imposed linear variation was assumed to vary continuously from zero at the initial station X/L = 0.4 to a maximum at X/L = 0.45 and then back to zero at X/L = 0.6. For comparison purposes first-order boundary-layer calculations were also made in which $\partial p/\partial x$ was assumed to be a function of x only by setting $u_i(x,y) = u_e(x)$, where u_e is the inviscid flow velocity tangent to the displacement body.

The computed skin friction and displacement body pressure distributions both with and without normal pressure gradients are shown in Figs. 13 and 14, respectively. It is observed in Fig. 13 that the rapid increase in the prescribed displacement thickness distribution results in a separated flow which extends from X/L = 0.41 to X/L = 0.49. Both the skin-friction and displacement body pressures show only minor changes due to the inclusion of an imposed normal pressure gradient; however comparison of the velocity profiles in Fig. 15 shows significant effects particularly in the outer part of the boundary layer. The x-location of these profiles is indicated on the prescribed perturbation mass flow distribution in Fig. 12. Figure 15 shows that the computed profiles blend smoothly with the prescribed linear variation in the inviscid velocity at the boundary-layer edge. Numerical tests were performed which indicated that the calculations are independent of where the outer boundary conditions are imposed provided this location is placed sufficiently far from the the wall. The variation across the boundary layer of the ratio of the pressure coefficient to that at the displacement body is shown in Fig. 16 in which the location of the boundary-layer edge is indicated on each of the pressure distributions. It is observed that signficant pressure variation occurs across the boundary layer in this model problem with the maximum variation being 40 percent at X/L = 0.45.

No numerical difficulties were encountered in obtaining the solution for this model problem utilizing this new inverse formulation for separated flows. The key feature of this formulation is that the equations have been written such that the boundary-layer solution is required to merge smoothly with the inviscid flow over the generalized displacement body as the boundary-layer edge is approached.

Work has been initiated on the Kooi transonic shock boundary-layer interaction utilizing the first-order version of the boundary-layer analysis described in this section. The boundary-layer was computed from the leading edge of the flat plate by using the direct mode (pressure prescribed) of this analysis. The result of this calculation provides the upstream flow conditions for the shock interaction problem. In addition this relatively straightforward calculation provides an opportunity to check the accuracy of the present formulation against a conventional finite-difference boundary-layer analysis. Figure 17 shows a comparison of these results with those obtained by using the UTRC ABLE (Analysis of the Boundary Layer Equations) code (Ref. 37) along with the available experimental data of Kooi (Ref. 24). In both of these boundary-layer calculations instantaneous transition was assumed to occur at 40 mm from the plate leading edge which corresponds to the streamwise location of the roughness strip used by Kooi in his experiment to induce transistion from laminar to turbulent flow. Figure 17(a) shows excellent agreement between the two boundary-layer predictions for the displacement thickness although both analyses somewhat underpredict the value of δ^* quoted by Kooi. Figure 17(b) shows that the computed skin friction distributions are in excellent agreement with each other and with the value obtained by Kooi at x = 426 mm, which he deduced from a Clauser velocity profile plot suitably corrected for compressibility. In addition excellent agreement is observed in Fig. 17(c) between the computed and measured velocity profile. This velocity profile is the same as that which was imposed in the inviscid calculation for the Kooi case, as was discussed previously.

Prior to a viscous analysis of the Kooi case, a comparison was made between the first-order version of the inverse boundary-layer formulation developed in the present effort and the previous method (Ref. 32) for the axisymmetric transonic shock induced separation case shown in Fig. 1. Although these two formulations are similar in overall approach they differ significantly in detail. Hence it was desired to make a comparison between these two approaches for the same input perturbation mass flow (Eq. 13) distribution which, in this case, was that deduced from the viscous-inviscid interation calculation for which the interacted pressure is shown in Fig. 1. The results obtained from these two inverse boundary-layer formulations are in good agreement thereby indicating that the first order version of the newly developed inverse boundary-layer formulation yields essentially the same results as the analysis used heretofore.

For the Kooi case the perturbation mass flow, given in Eq. (13) and prescribed for the first-order inverse boundary-layer analysis, was computed from the distribution of displacement thickness deduced experimentally by Kooi along with the experimental wall pressure distribution which was used to find $\rho_e u_e$ from one-dimensional isentropic flow theory. Kooi's experimental δ_*-distribution is shown in Fig. 18(a) with the streamwise position of the normal shock also indicated. After the inverse boundary-layer computation was completed and $\rho_e u_e$ deduced from the solution, the displacement thickness was then computed from the prescribed perturbation mass flow $m = \rho_e u_e \delta^*$ and is shown in Fig. 18(a). Even though the present calculation overpredicted the pressure by 10 percent as will be discussed below for Fig. 18(b), this inaccuracy has only a small effect on the product $\rho_e u_e$ since it is O(1) for transonic speeds. Hence the close agreement as shown in Fig. 18(a) of the computed displacement thickness with that determined experimentally by Kooi indicates that the present analysis was made for the experimental displacement thickness expressed in terms of the perturbation mass flow parameter, m.

Comparison of the computed and experimental wall pressure and skin friction distributions are shown in Figs. 18(b) and 18(c), respectively. It is observed that the present analysis overpredicts the experimental wall pressure and correspondingly this stronger adverse pressure gradient results in a larger separated flow region than that observed experimentally by Kooi as can be seen in Fig. 18(c). Similarly the present analysis over predicts the boundary-layer thickness as shown in Fig. 19. At the present time it is not clear whether the differences between the theory and experiment shown in Figs. 18 and 19 are attributable to the use of an algebraic eddy viscosity model or the lack of normal pressure gradient effects in the calculation. In the next phase of this contract, work will focus on further development of the inviscid stream function analysis so that the input for the viscous analysis will include this effect.

CONCLUDING REMARKS

A viscous-inviscid flow interaction model has been developed for the strong interaction which occurs when a transonic normal shock impinges on a turbulent boundary-layer. The case of interest in the present study is where the shock is of sufficient strength to result in boundary-layer separation. In the phase of this work just completed, the viscous and inviscid analyses have been separately developed and demonstrated to be capable of analysis in this transonic flow regime. In the next phase of these two analyses will be iteratively coupled together for the prediction of transonic shock induced separated flow.

ACKNOWLEDGEMENTS

The principal investigators in the present contract acknowledge the cooperation given in this project by the NASA-Langley Research Center in granting permission to Dr. M. Hafez to perform the stream function calculations reported herein on the NASA-Langley computer system. In addition, the first author acknowledges the interest and suggestions made by Dr. M. J. Werle of UTRC; the second author acknowledges the help of D. Lovell and C. Glumbert of the NASA-Langley Research Center in the inviscid computations.

REFERENCES

1. Viegas, J. R. and C. C. Horstman: Comparison of Multiequation Turbulence Models for Several Shock Boundary-Layer Interaction Flows. AIAA Journal, Vol. 17, No. 8, August 1979.

2. Johnson, D. A., C. C. Horstman and W. D. Bachalo: A Comprehensive Comparison Between Experiment and Predictions for a Transonic Turbulent Separated Flow. AIAA Paper No. 80-1407, July 1980.

3. Carter, J. E.: Numerical Solutions of the Navier-Stokes Equations for the Supersonic Laminar Flow Over a Two-Dimensional Compression Corner. NASA TR-R-385, 1972.

4. Werle, M. J. and V. N. Vatsa: New Method for Supersonic Boundary Layer Separation. AIAA Journal, Vol. 12, pp. 1491-97, 1974.

5. Vatsa, V. N., J. E. Carter and R. C. Swanson: Comparison of Solutions of the Navier-Stokes and Interacting Boundary-Layer Equations for Separated Turbulent Flow. To be presented at the ISCEM Intl. Conference on Computational Method and Experimental Measurements, Washington, D.C., June 30-July 2, 1982.

6. Bauer, F., P. Garabedian, D. Korn and A. Jameson: Supercritical Wing Sections, II. Springer-Verlag Publisher, 1975.

7. Carlson, L. A.: TRANDES: A Fortran Program for Transonic Airfoil Analysis or Design. NASA CR-2821, June 1977.

8. Catherall, D. and K. W. Mangler: The Integration of the Two-Dimensional Laminar Boundary-Layer Equations Past the Point of Vanishing Skin Friction. J. Fluid Mech., Vol. 26, Pt. 1, Sept. 1966.

9. Carter, J. E.: Solutions for Laminar Boundary Layers with Separation and Reattachment. AIAA Paper No. 74-583, June 1974.

10. Klineberg, J. M. and J. L. Steger: On Laminar Boundary-Layer Separation. Paper No. 74-94, January 1974.

11. Carter, J. E.: Inverse Boundary Layer Theory and Comparison with Experiment. NASA TP-1208, Sept. 1978.

REFERENCES (Cont'd)

12. Carter, J. E.: A New Boundary-Layer Inviscid Iteration Technique for Separated Flow. AIAA Paper No. 79-1450, AIAA 4th Computational Fluid Dynamics Conference. Williamsburg, VA, July 23-24, 1979.

13. Kwon, O. K. and R. H. Pletcher: Prediction of Incompressible Separated Boundary Layers Including Viscous-Inviscid Interaction, J. Fluids Eng., Vol. 101, pp. 466-472, Dec. 1979.

14. Kuhn, G. D.: An Improved Interaction Method for Exhaust Nozzle Boattail Flows. AIAA Paper No. 80-0197, January 1980.

15. Whitfield, D. L., T. W. Swafford and J. L. Jacocks: Calculation of Turbulent Boundary Layers with Separation, Reattachment and Viscous-Inviscid Interaction. AIAA Paper No. 80-1439, July 1980.

16. Werle, M. J. and J. M. Verdon: Viscid/Inviscid Interaction for Symmetric Trailing Edges. Naval Air Systems Command Contract N00019-78-C-0604, November 1979.

17. LeBalleur, J. C.: Strong Matching Method for Computing Transonic Viscous Flows Including Wakes and Separations. Lifting Airfoils, La Recherche Aerospaticle, No. 1981-3, English edition, 1981.

18. Wigton, Laurence B and Holt, Maurice: Viscous-Inviscid Interaction in Transonic Flow. AIAA 5th Computational Fluid Dynamics Conference, June 22-23, 1981.

19. Carter, J. E.: Development of a Prediction Method for Transonic Shock Induced Separated Flow. Office of Naval Research Contract N00014-81-C-0381.

20. South, J. C., Jr. and A. Jameson: Relaxation Solutions for Inviscid Axisymmetric Transonic Flow Over Blunt or Pointed Bodies. AIAA Computational Fluid Dynamics Conference, Palm Springs, CA, pp. 8-17, July 1973.

21. Green, L. L.: Conservation Full-Potential Calculations for Axisymmetric, Transonic Flow. AIAA Paper No. 81-1204, June 1981.

22. Melnik, R. E.: Turbulent Interactions on Airfoils at Transonic Speeds-Recent Developments. Presented at Computation of Viscous-Inviscid Interactions, AGARD Conference Preprint of Viscous-Inviscid Interactions, AGARD Conference Preprint No. 291, 1981.

REFERENCES (Cont'd)

23. Lighthill, M. J: On Boundary Layers and Upstream Influence II, Supersonic Flows Without Separation. Proceedings Roy. Soc., Series A, Vol. 217, 1953.

24. Kooi, J. W.: Influence on Free-Stream Mach Number on Transonic Shock Wave Boundary Layer Interaction. NLR MP 78013 U, National Aerospace Laboratory, Netherlands, 1978.

25. East, L. F.: The Application of a Laser Anemometer to the Investigation of Shock Wave Boundary Layer Interactions. AGARD-CP-193, 1976.

26. Melnik, R. E. and B. Grossman: Analysis of the Interaction of a Week Normal Shock Wave with a Turbulent Boundary Layer. AIAA Paper No. 74-598, 1974.

27. Adamson, T. C., Jr. and A. Feo: Interaction Between a Shock Wave and a Turbulent Boundary Layer in Transonic Flow. SIAM J. Appl., Vol. 29, 1975.

28. Messiter, A. F.: Interaction Between a Normal Shock Wave and Turbulent Boundary Layer at High Transonic Speeds, Pt. I: Pressure Distribution NASA CR-3194, 1979.

29. LeBalleur, J. C. R. Peyret and H. Viviand: Numerical Studies in High Reynolds Number Aerodynamics. Journal of Computers and Fluids, Vol. 8, No. 1, March 1980.

30. East, L. F.: A Representation of Second-Order Boundary Layer Effects in the Momentum Integral Equation and in Viscous-Inviscid Interactions. RAE Technical Report 81002, 1981.

31. Hafez, M. M. and D. Lovell: Numerical Solution of the Transonic Stream Function Equation. AIAA 5th Computational Fluid Dynamics Conference, June 22-23, 1981.

32. Carter, J. E.: Viscous-Inviscid Interaction Analysis of Transonic Turbulent Separated Flow. AIAA Paper No. 81-1241, 1981.

33. Steger, J. L. and H. Lomax: Calculation of Inviscid Shear Flow Using a Relaxation Method for the Euler Equations. Aerodynamic Analyses Requiring Advanced Computers, NASA SP-341, Pt. II, pp. 811-838, March 4-6, 1975.

34. Coles, D.: The Law of the Wake in the Turbulent Boundary Layer. J. Fluid Mech., Vol. 1, Pt. 2, pp. 191-226, July 1956.

REFERENCES (Cont'd)

35. Hafez, M. M., J. C. South and E. M. Murman: Artificial Compressibility Mehtods for Numerical Solution of Transonic Full-Potential Equation. AIAA Paper No. 78-1148, July 1978.

36. Carter, J. E. and Vatsa, V. N.: Analysis of Separated Boundary Layer Flows, Presented at the Eighth International Conference on Numerical Methods in Fluid Dynamics, Aachen, W. Germany, June 28-July 2, 1982.

37. Edwards, D. E., J. E. Carter, M. J. Werle: Analysis of the Boundary Layer Equations Including a New Composite Coordinate Transformation - the ABLE Code, UTRI Report 81-30, May 1982.

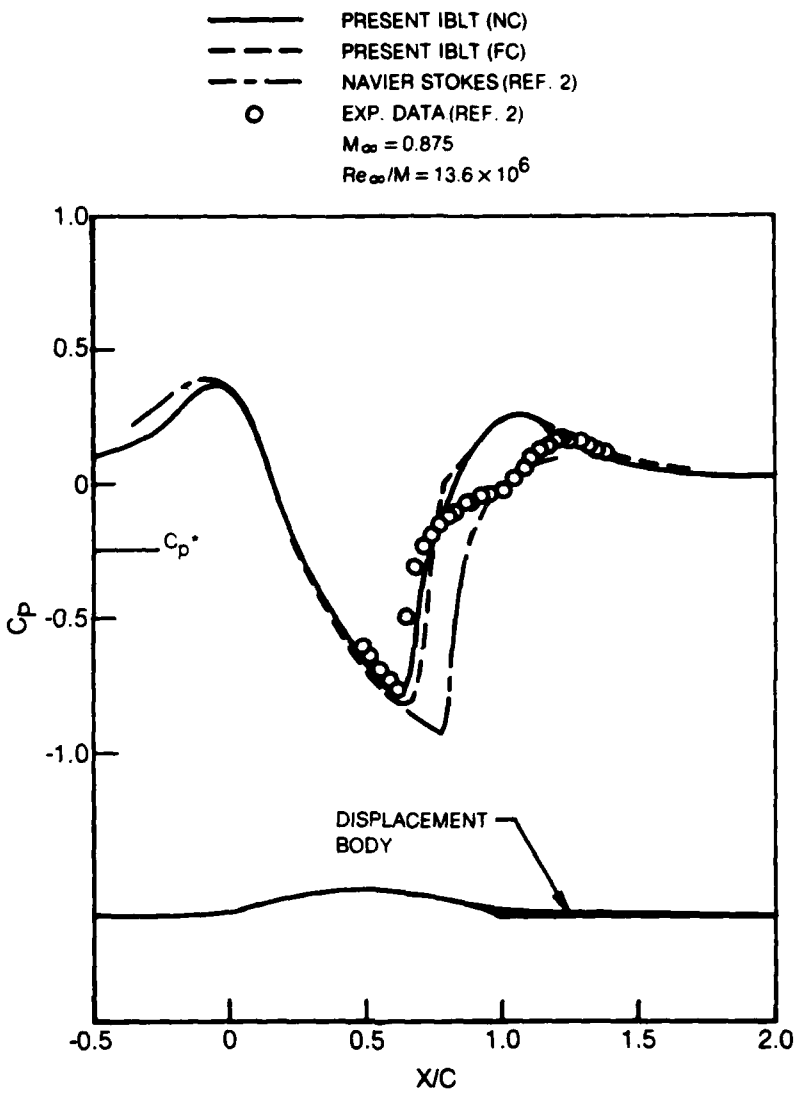

Fig. 1 Transonic pressure distributions on axisymmetric body

81-5-137-9

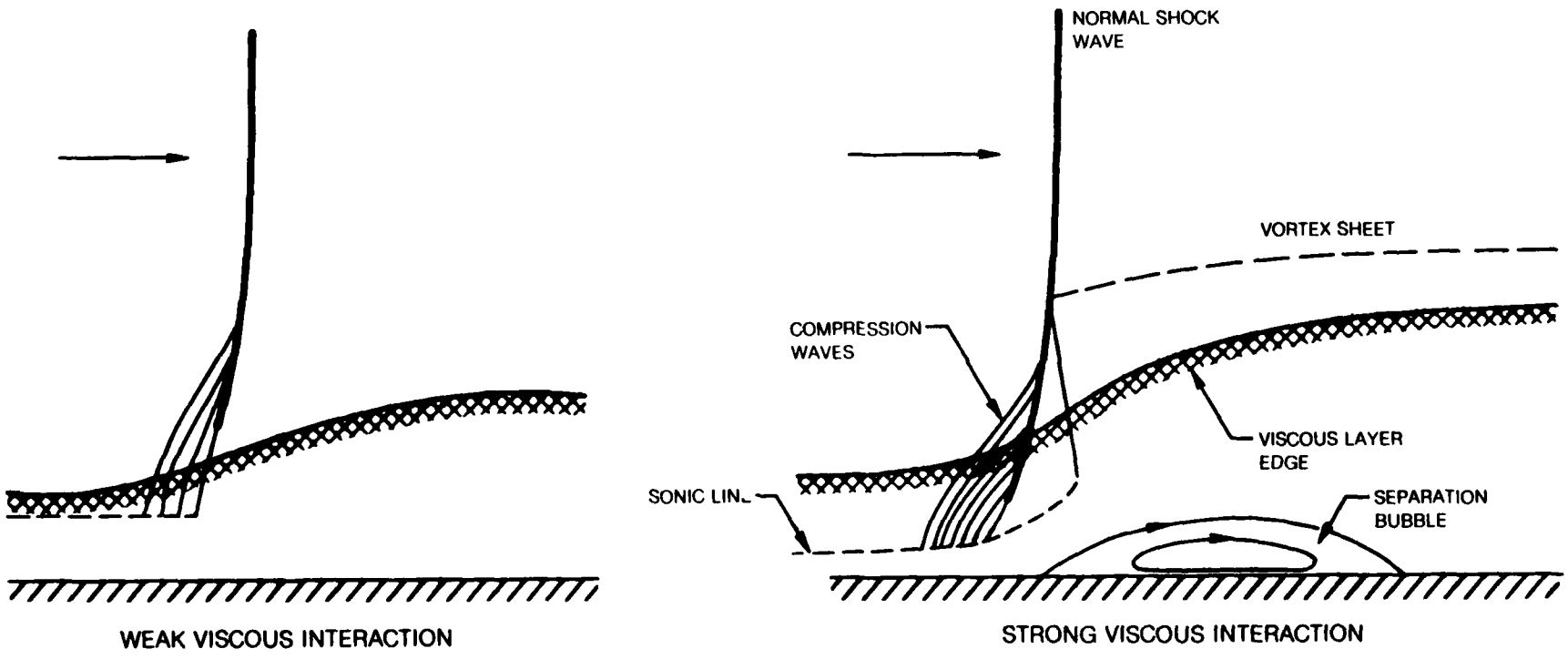

Fig. 2 Interaction of normal shock wave and turbulent boundary layer on a flat plate

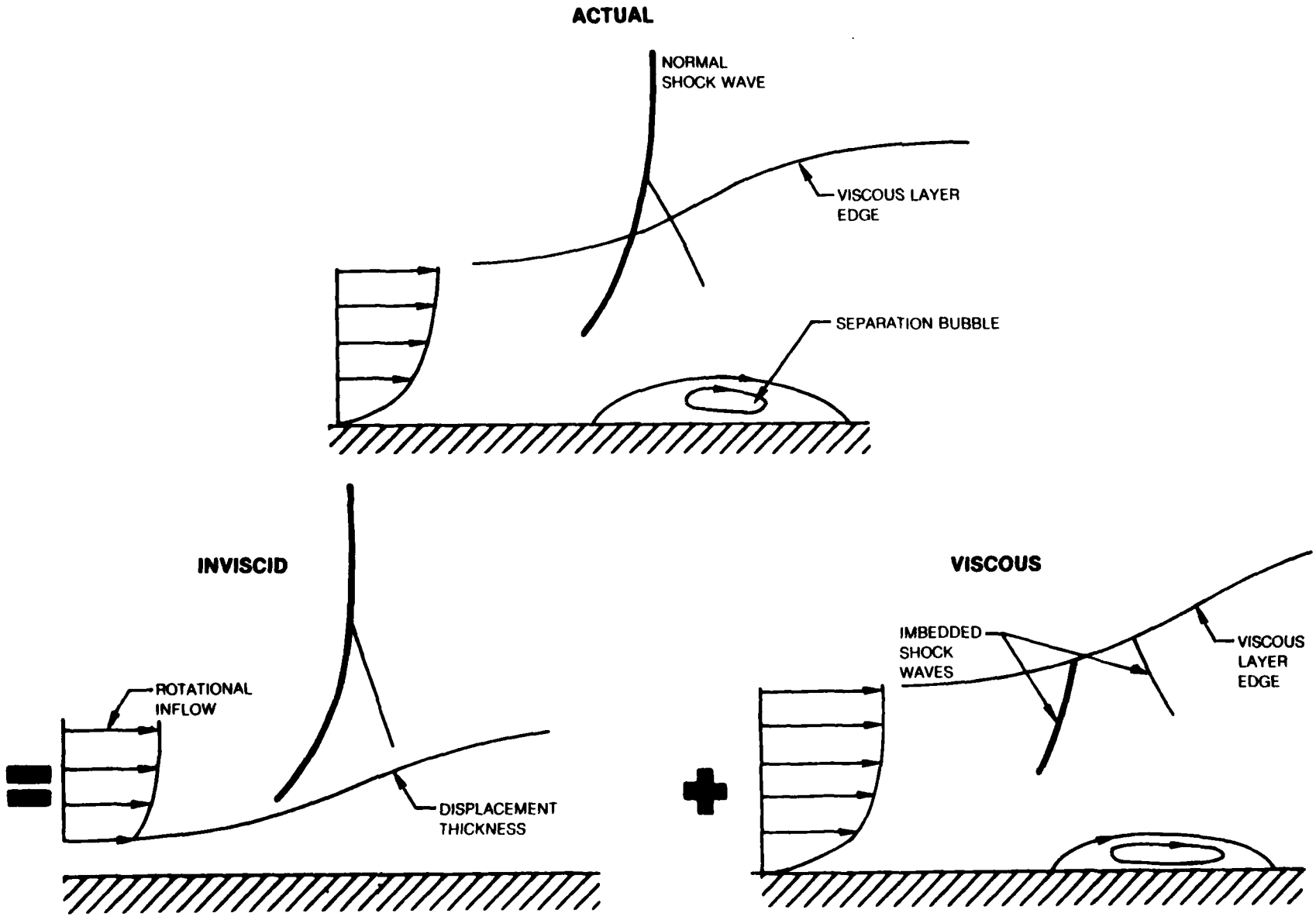

Fig. 3 Strong viscous interaction flow model

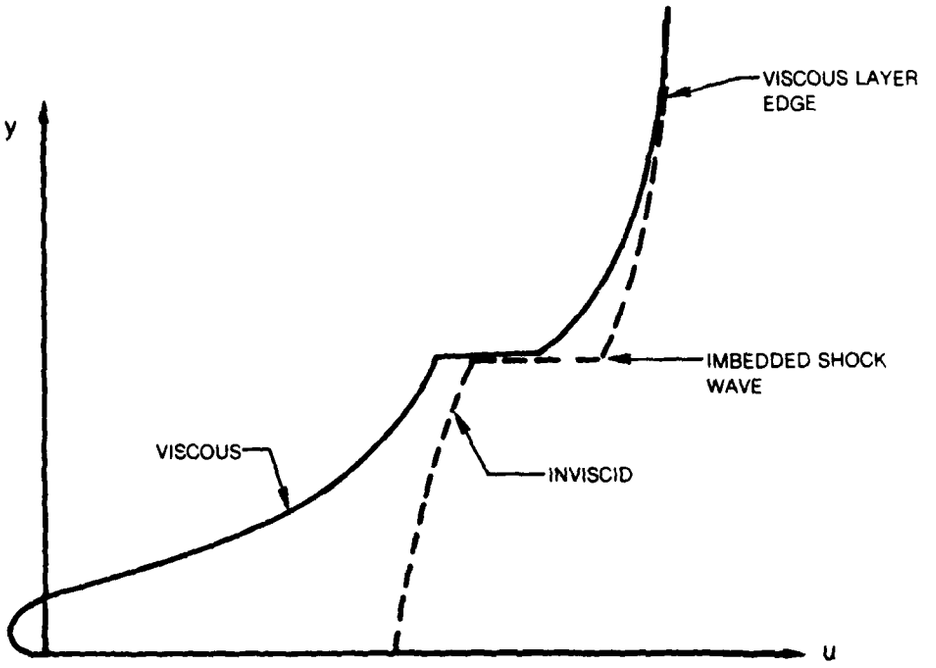

Fig. 4 Viscous-inviscid matching of velocity profiles

80-9-29-6

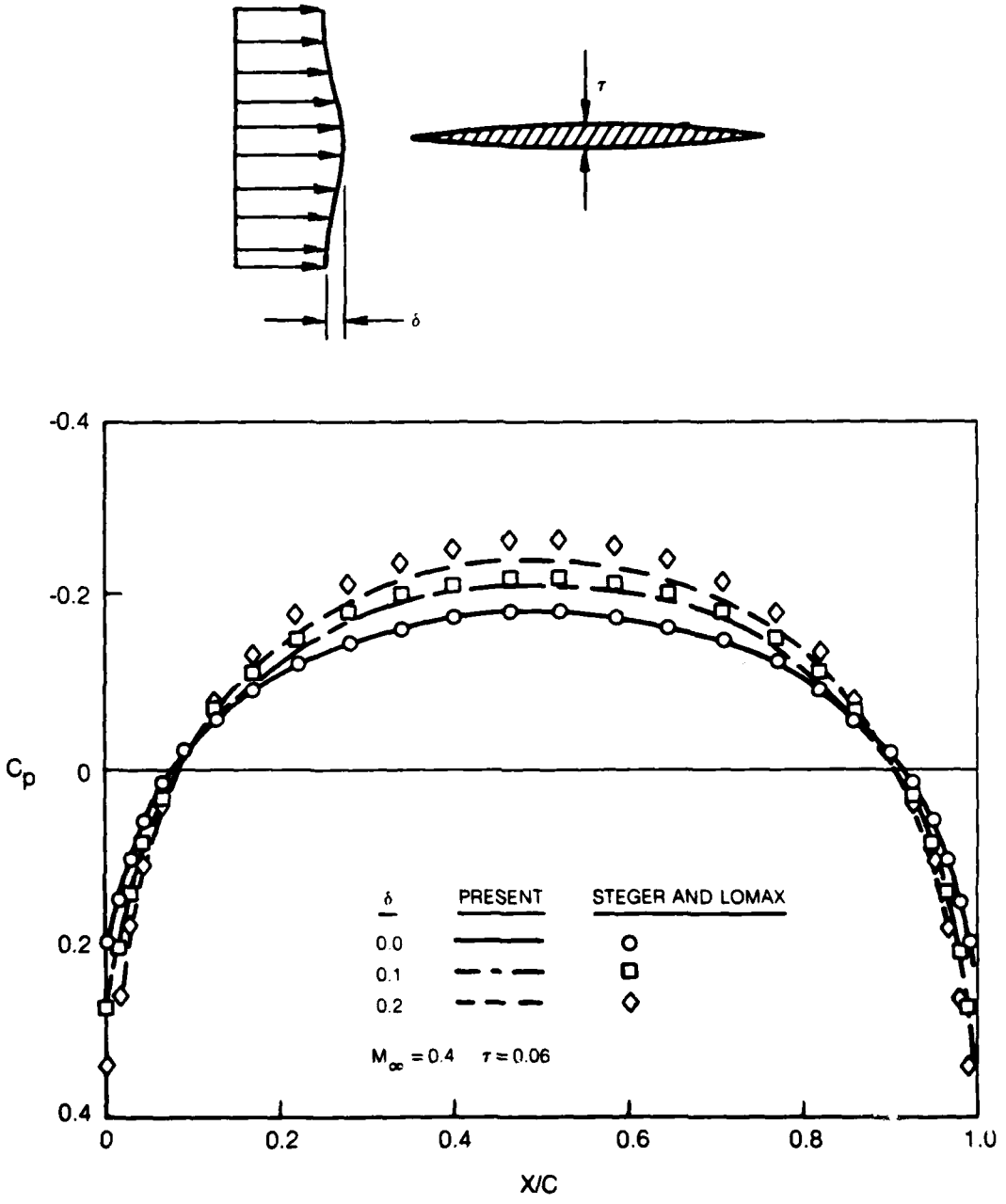

Fig. 5 Pressure distributions over parabolic arc airfoil with accelerated and heated incoming profiles

82-3-57-1

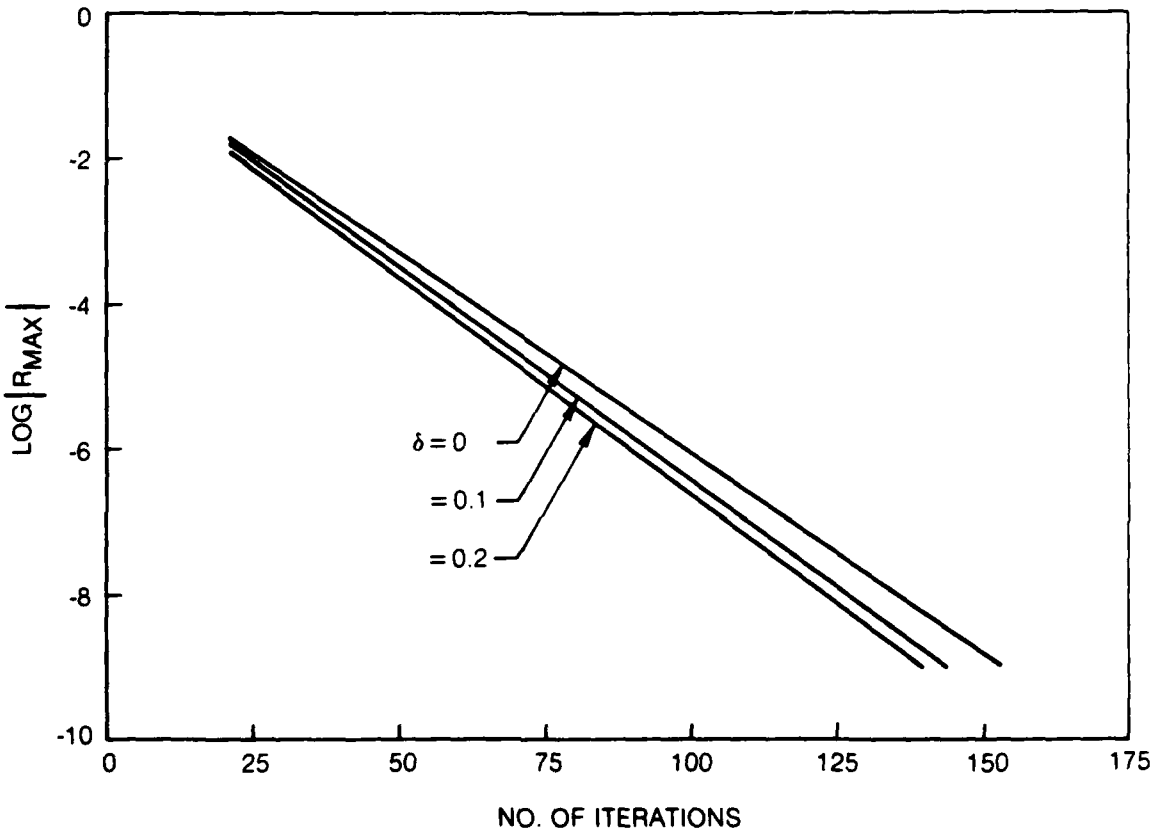

Fig. 6 Convergence history for analysis of accelerated flow over parabolic arc airfoil

82-3-57-2

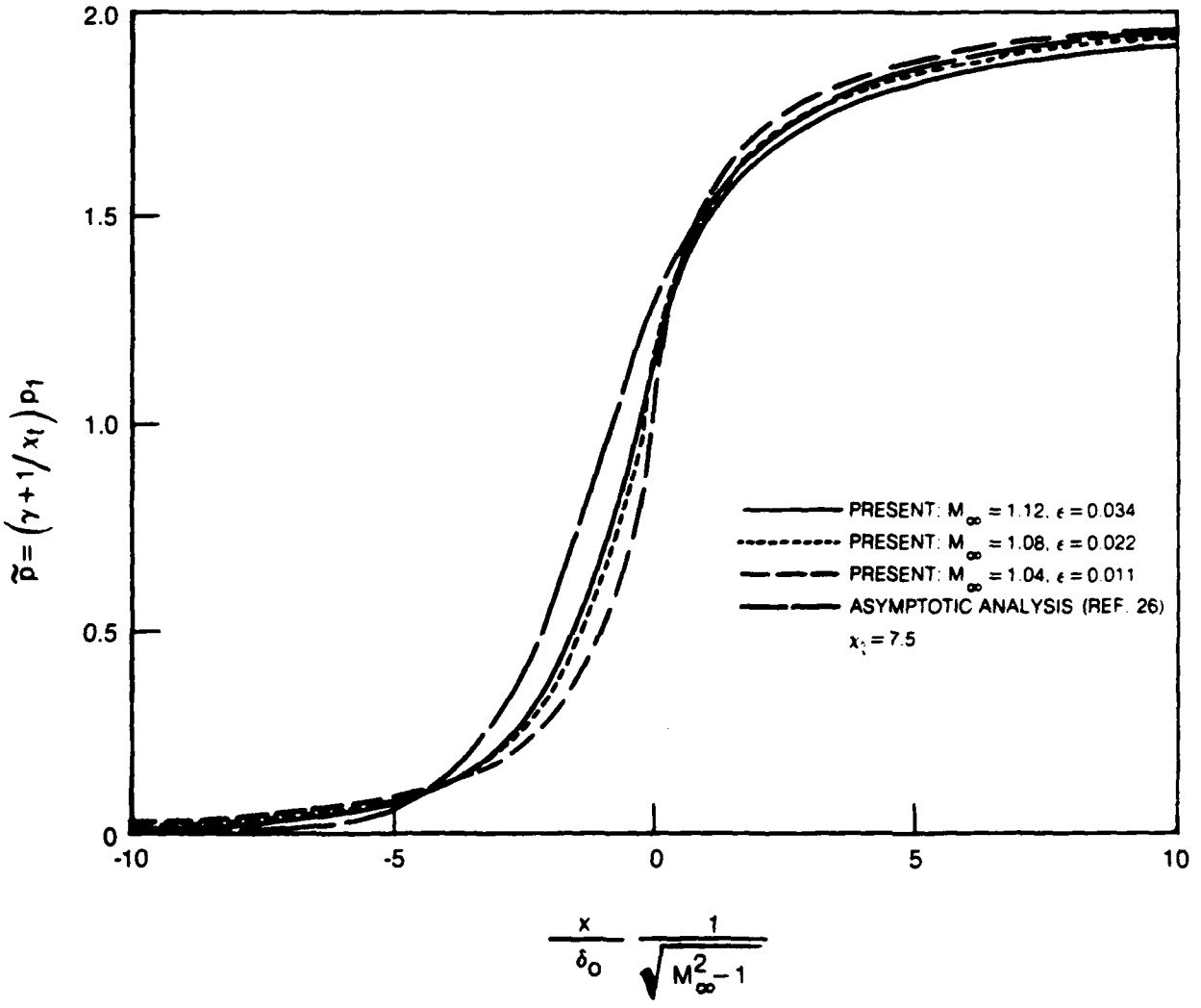

Fig. 7 Comparison of present solution with asymptotic analysis for transonic normal shock, inviscid rotational flow interaction

82-9-46-1

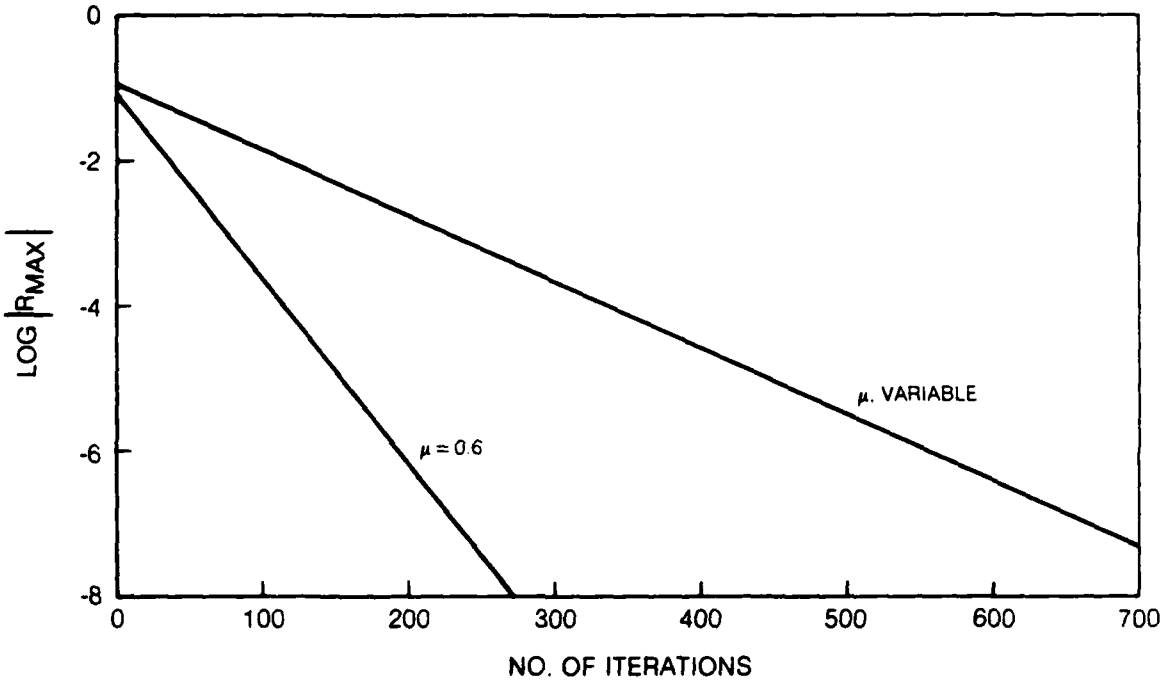

Fig. 8 Convergence history for transonic flow case

82-3-57-4

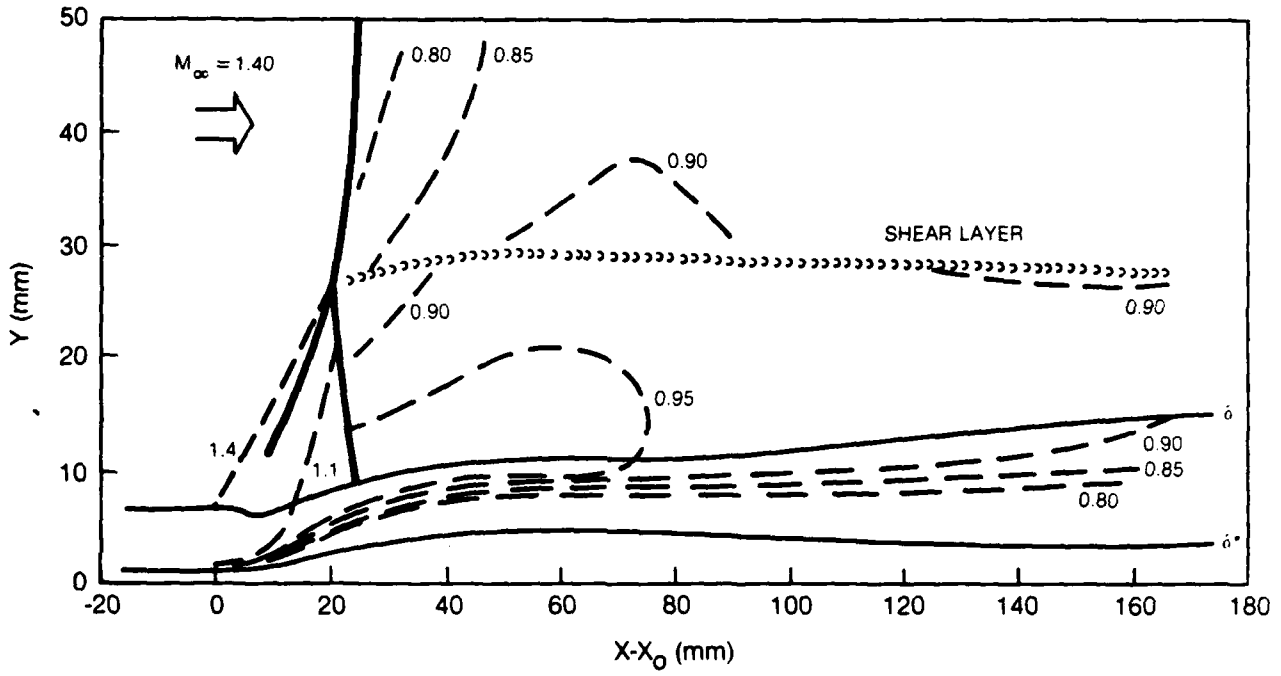

Fig. 9 Flow structure of normal shock-wave boundary-layer interaction deduced from experimental measurements (Kooi)

82-3-57-13

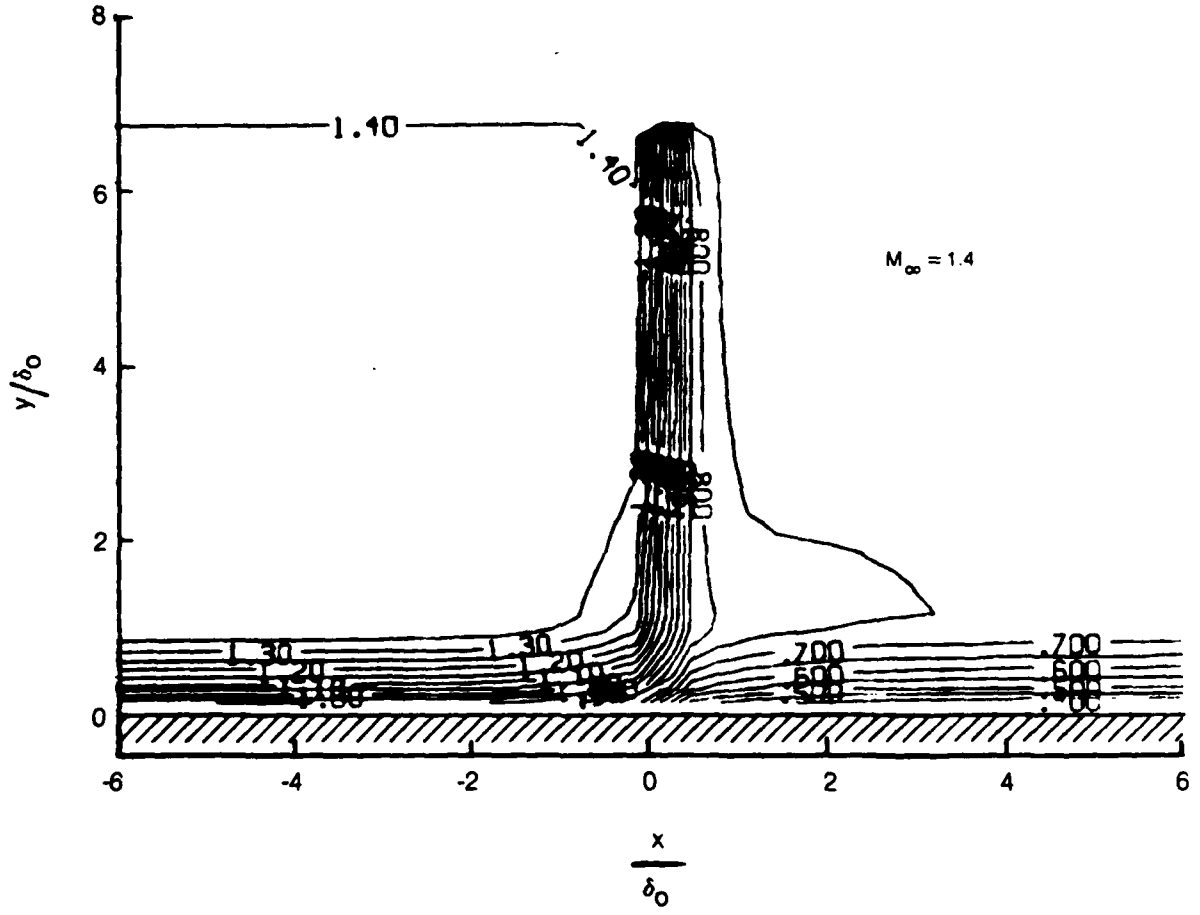

Fig. 10 Mach contours for transonic normal shock inviscid, rotational flow interacton — no displacement thickness

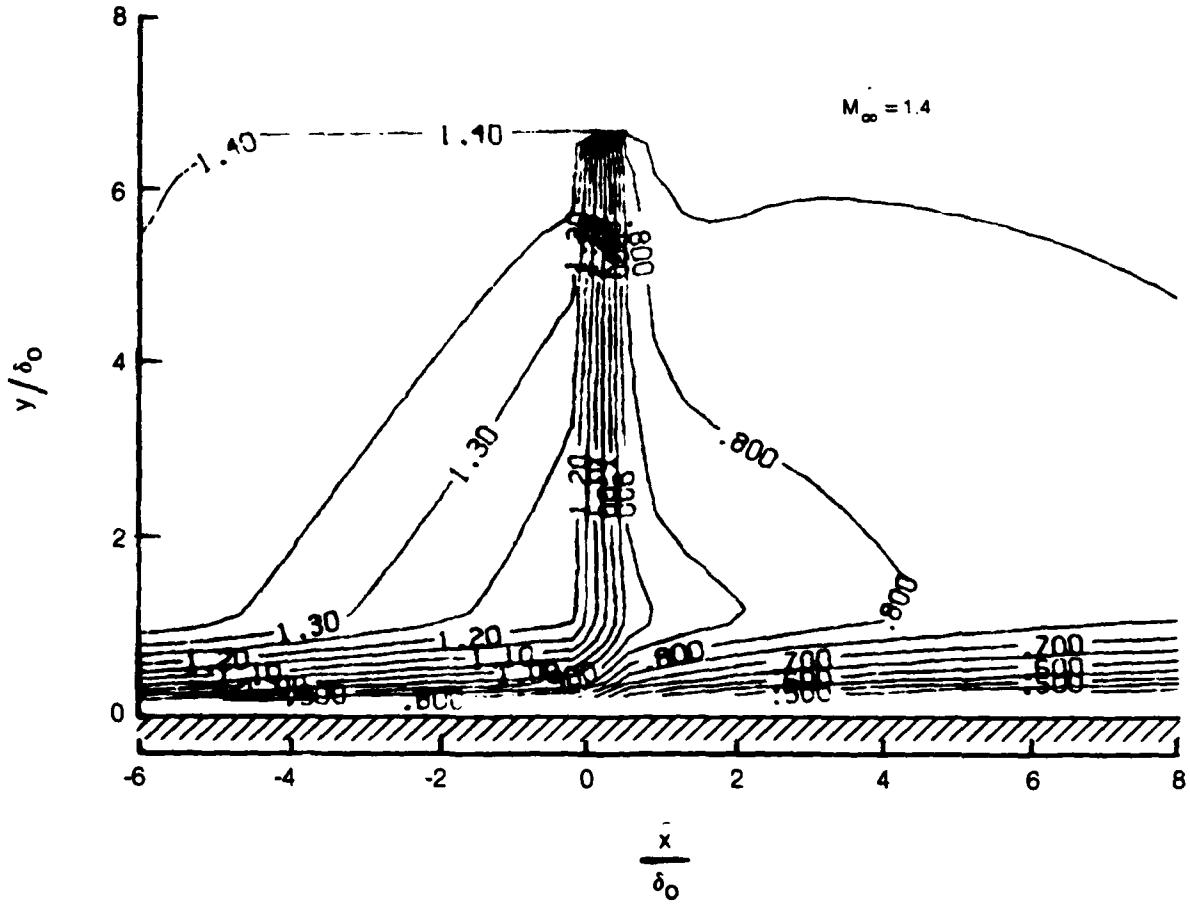

Fig. 11 Mach contours for transonic normal shock inviscid, rotational flow interaction — includes displacement thickness

82-9-46-8

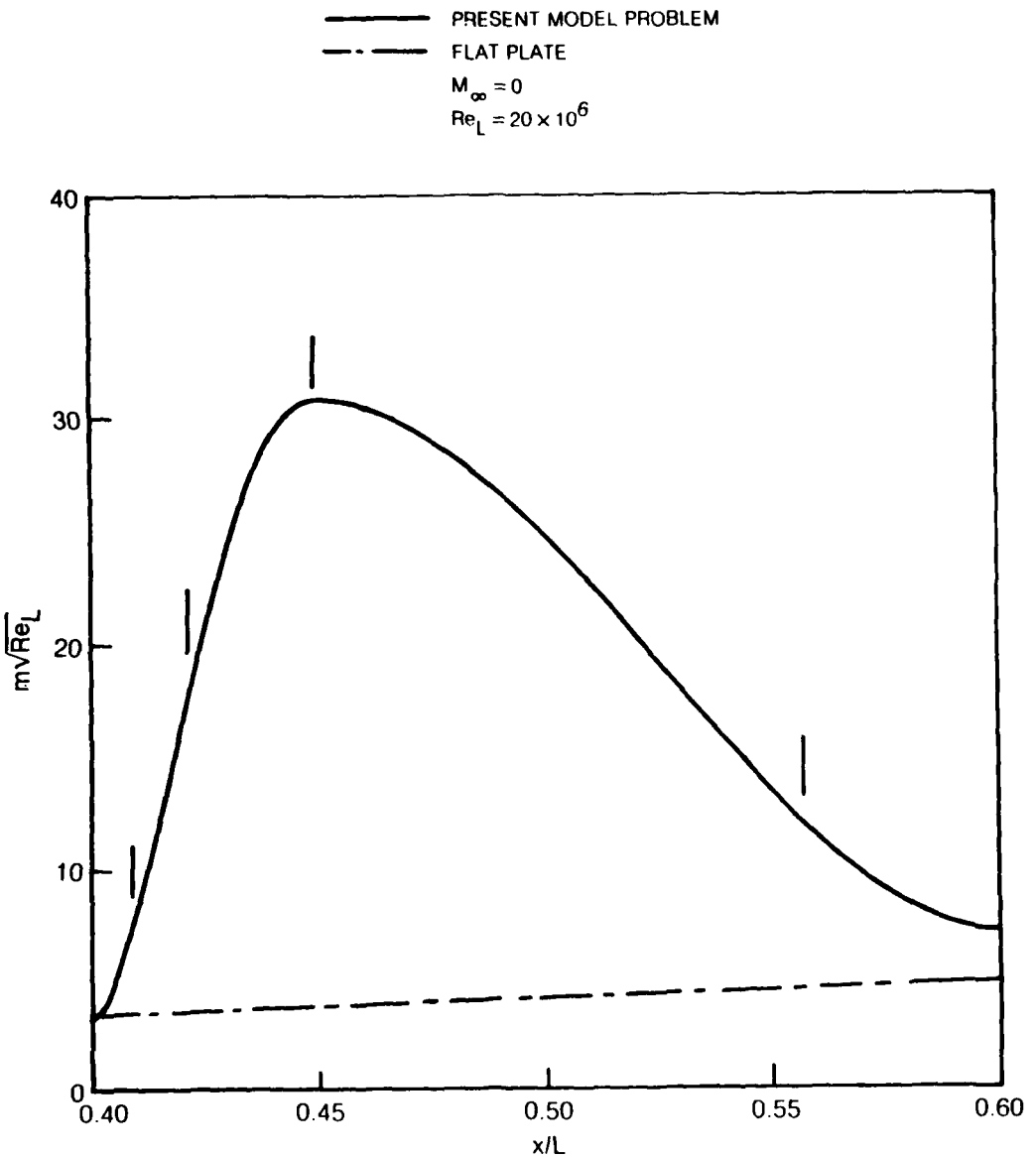

Fig. 12 Prescribed distribution of perturbation mass flow

82-3-67-5

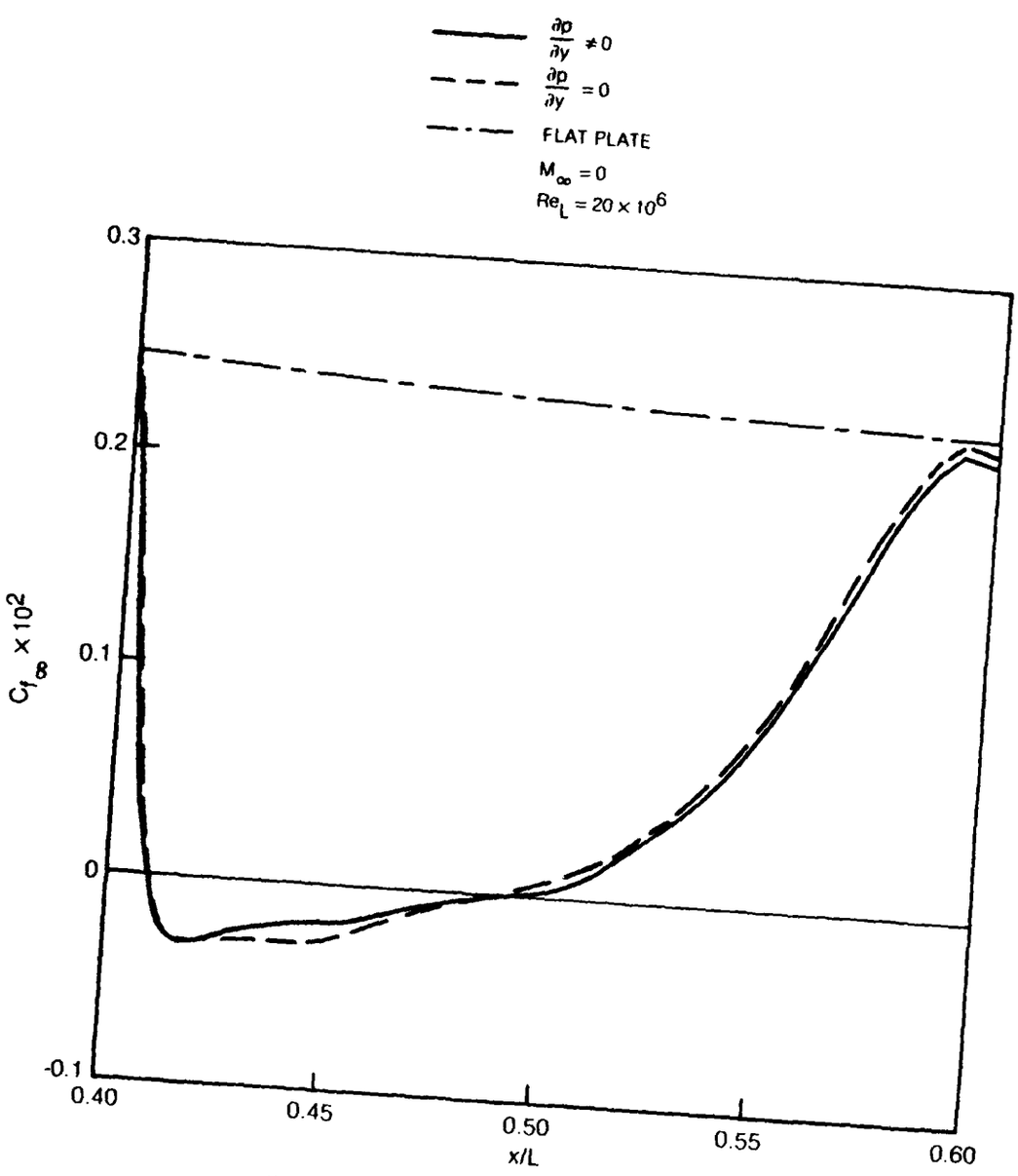

Fig. 13 Skin friction distributions

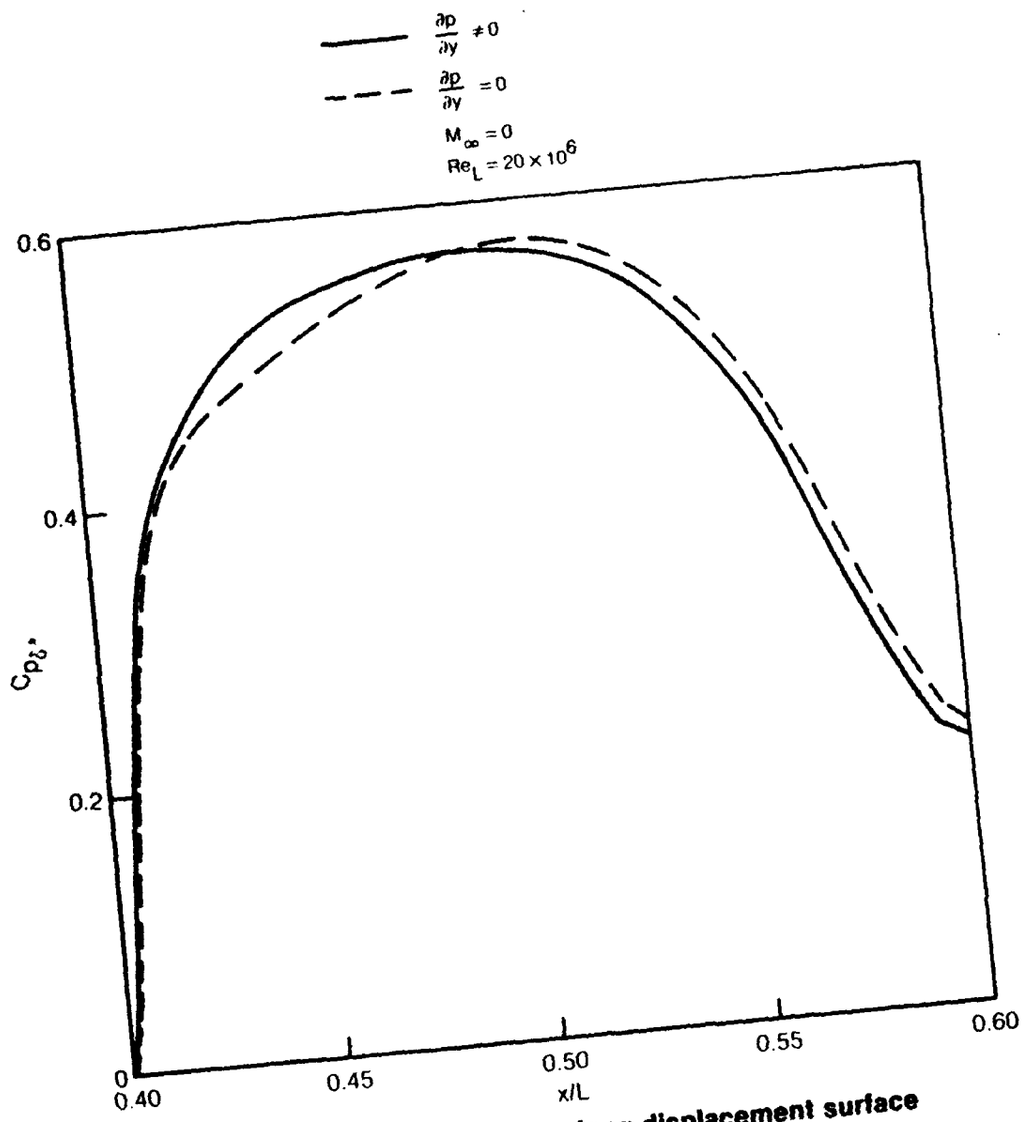

Fig. 14 Pressure distributions along displacement surface

82-3-57-7

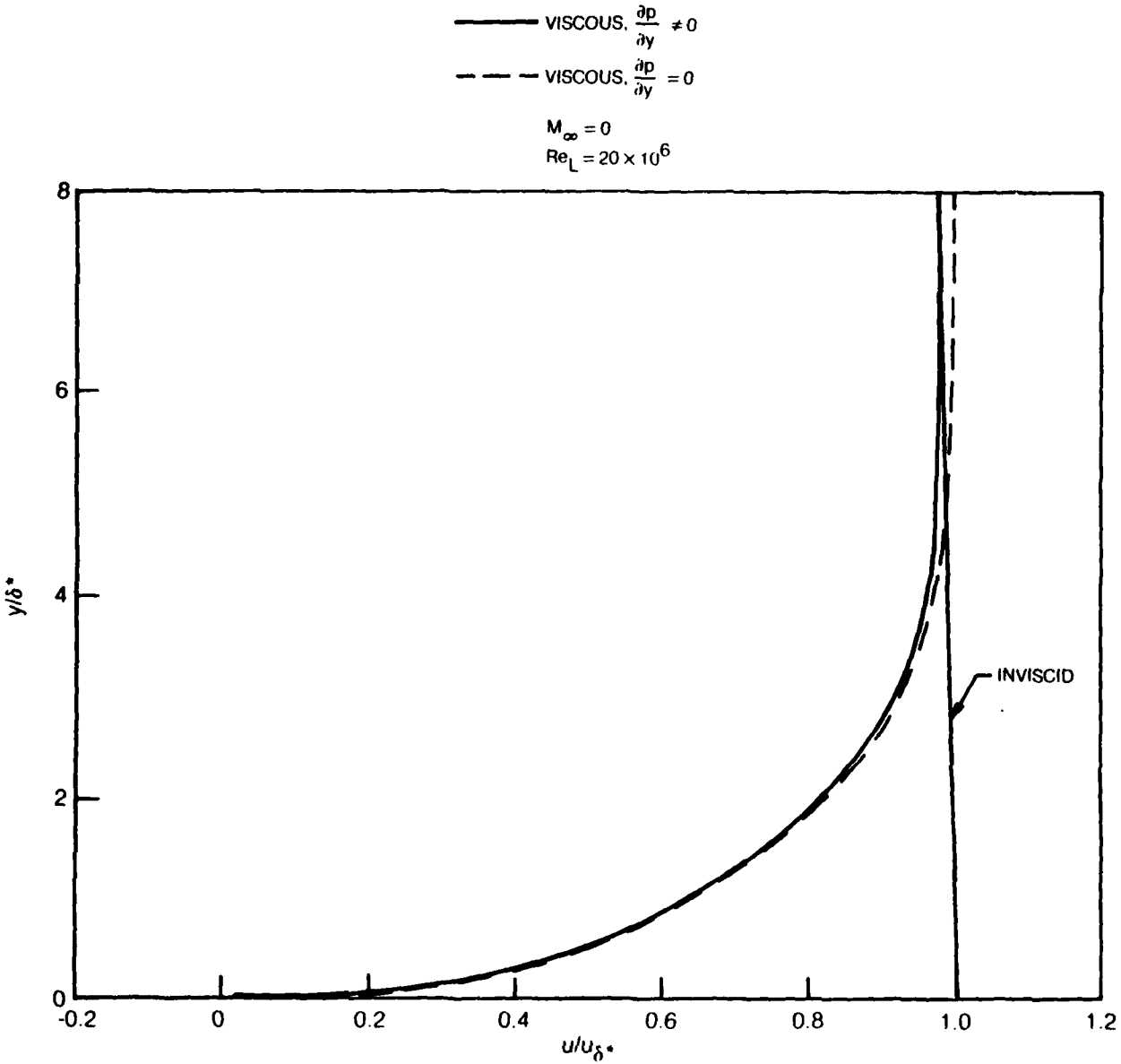

Fig. 15 Velocity profiles
a) x/L = 0.410

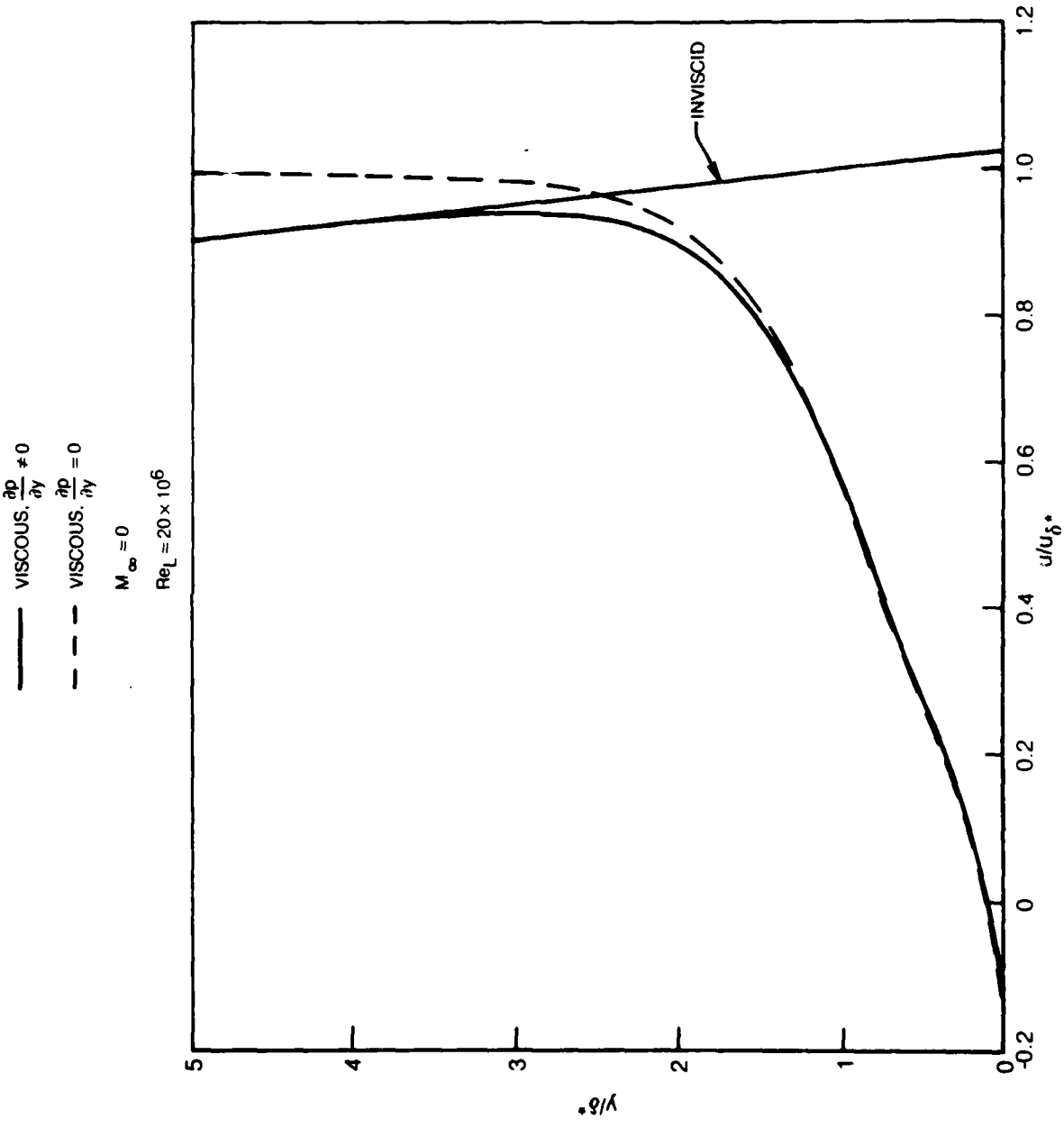

Fig. 15 Velocity profiles
b) x/L = 0.422

82-3-57-9

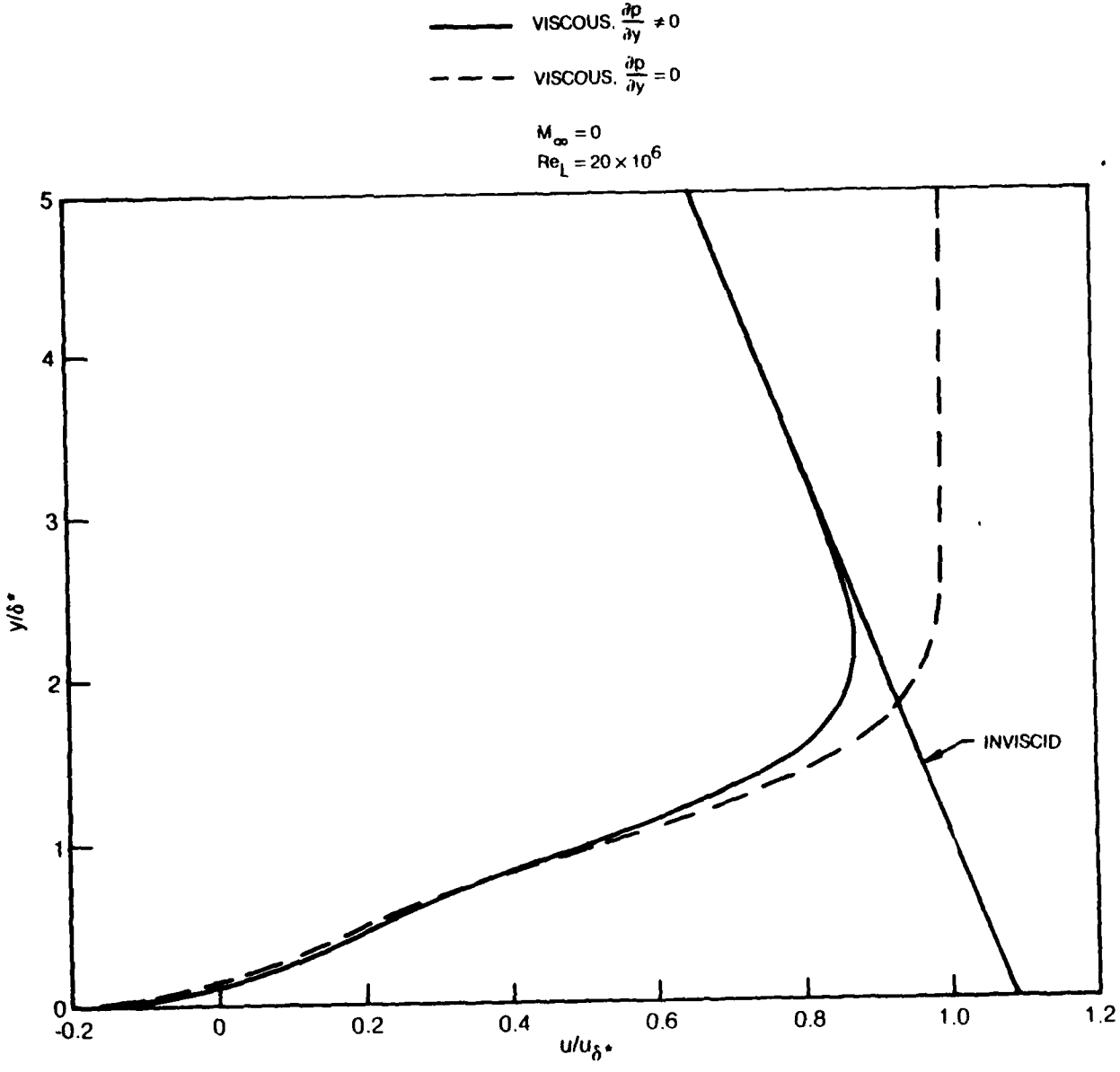

Fig. 15 Velocity profiles
c) x/L = 0.450

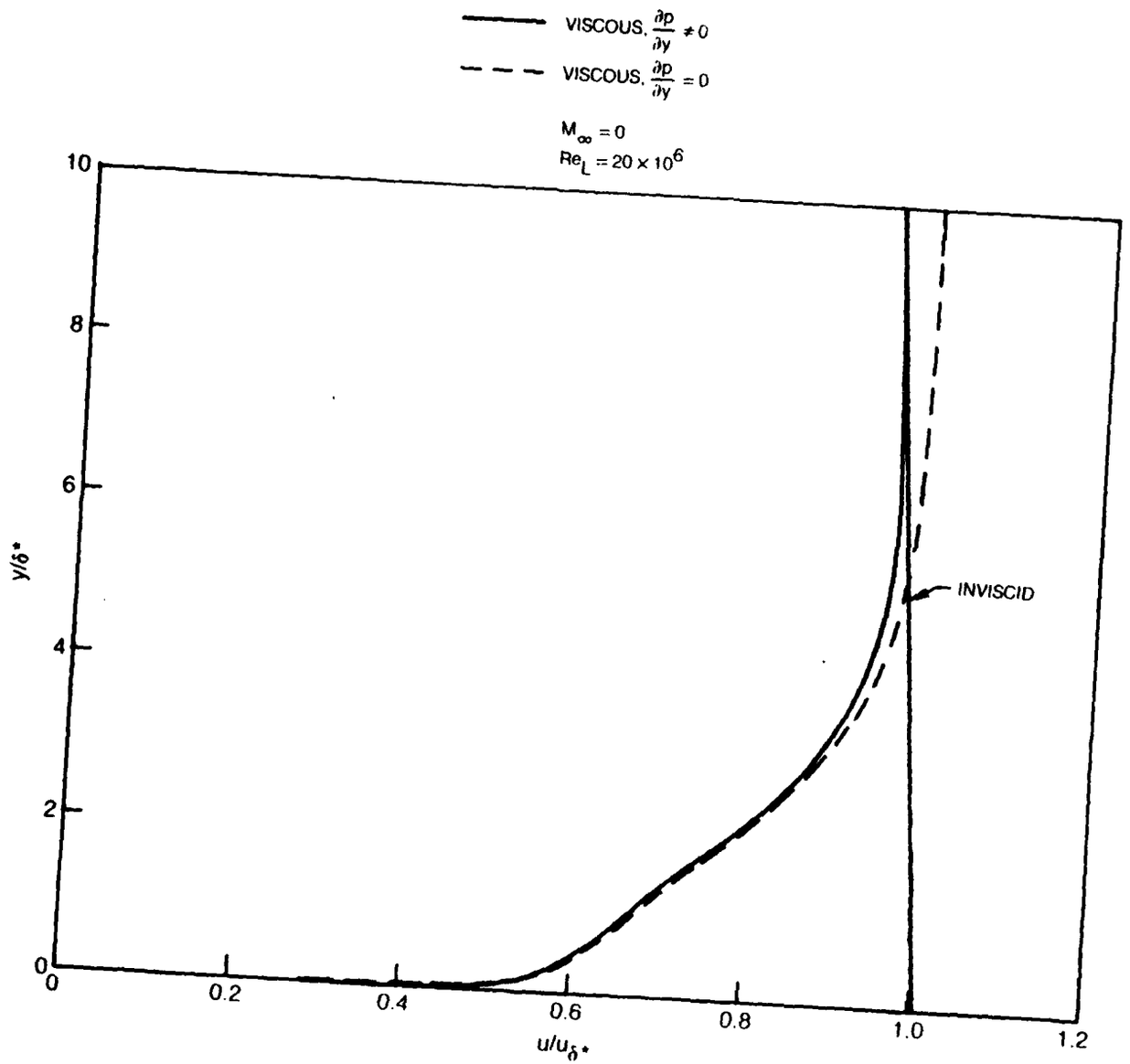

Fig. 15 Velocity profiles
d) x/L = 0.558

82-3-57-11

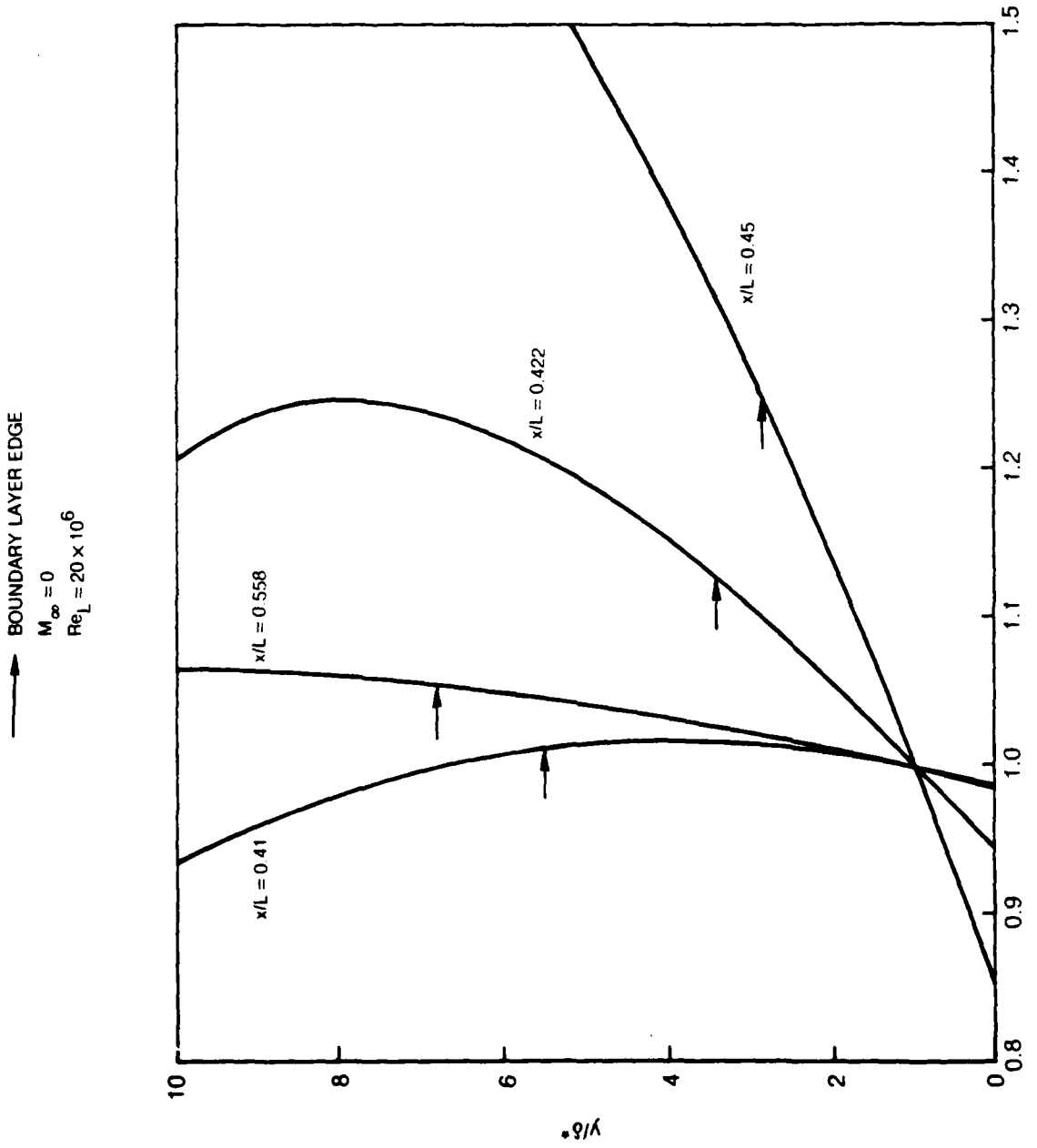

Fig. 16 Variation of pressure across boundary layer

82-3-57-12

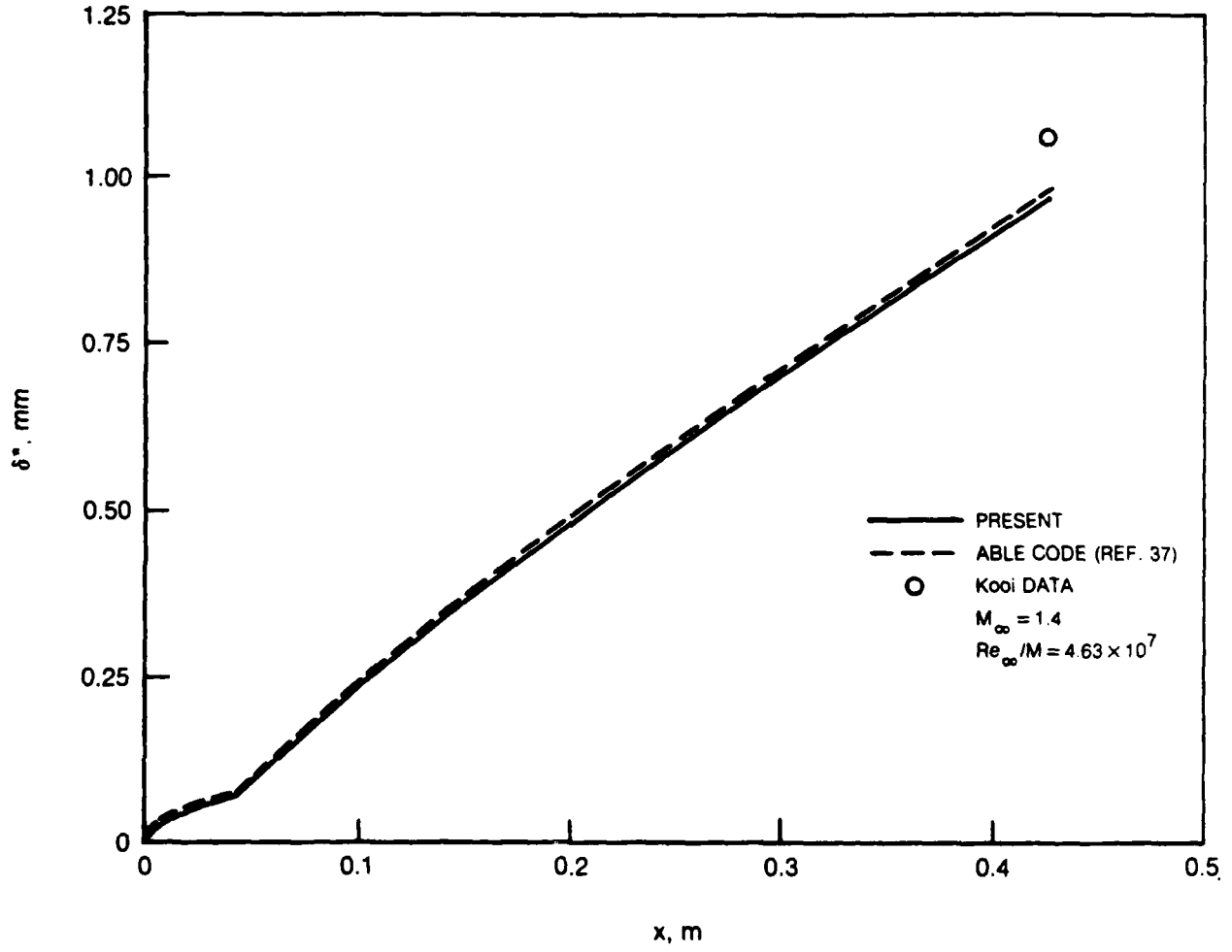

Fig. 17 Comparison of present boundary layer analysis with ABLE code and experimental data a) Displacement thickness

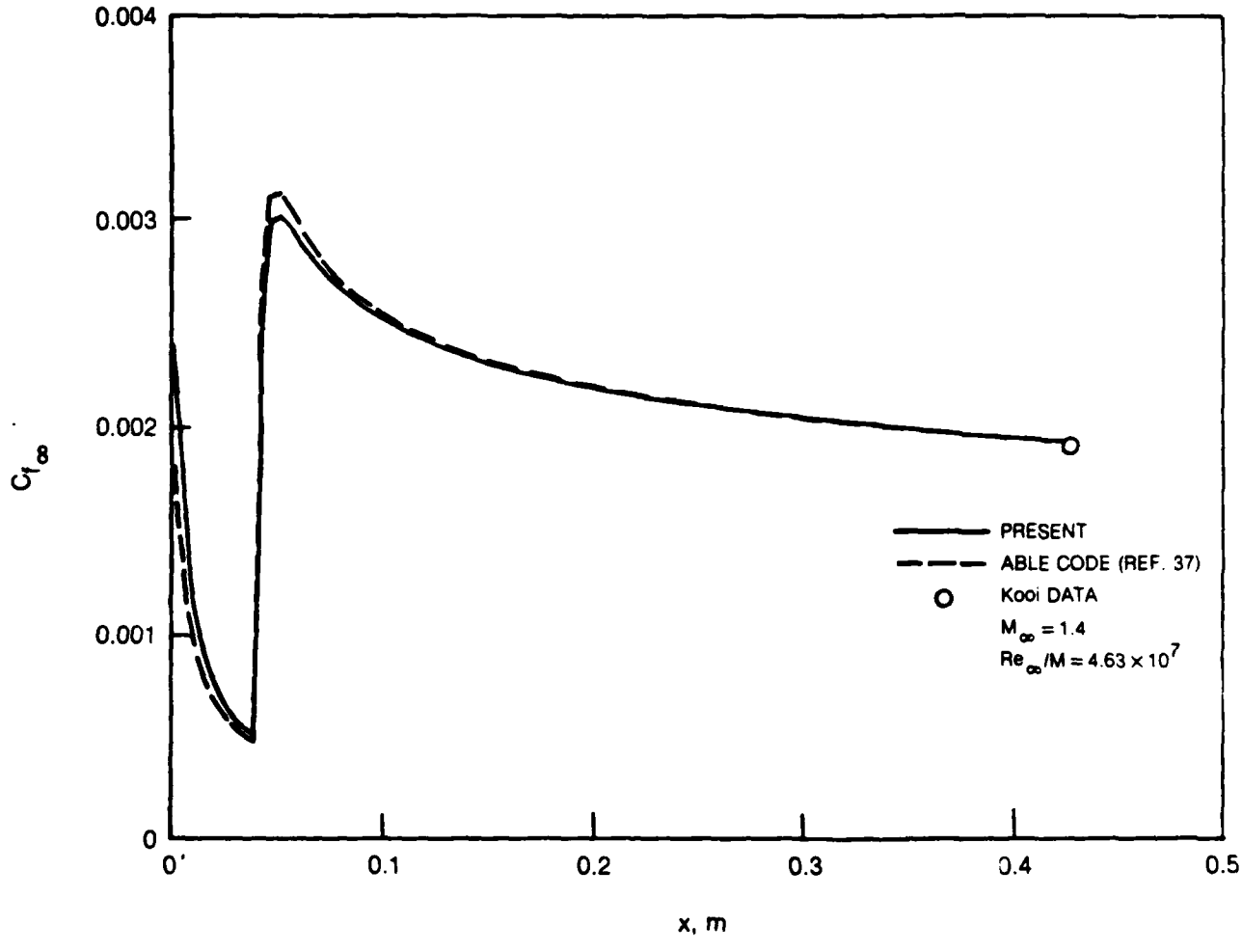

Fig. 17 Comparison of present boundary layer analysis with ABLE code and experimental data b) Skin friction

82-9-46-2

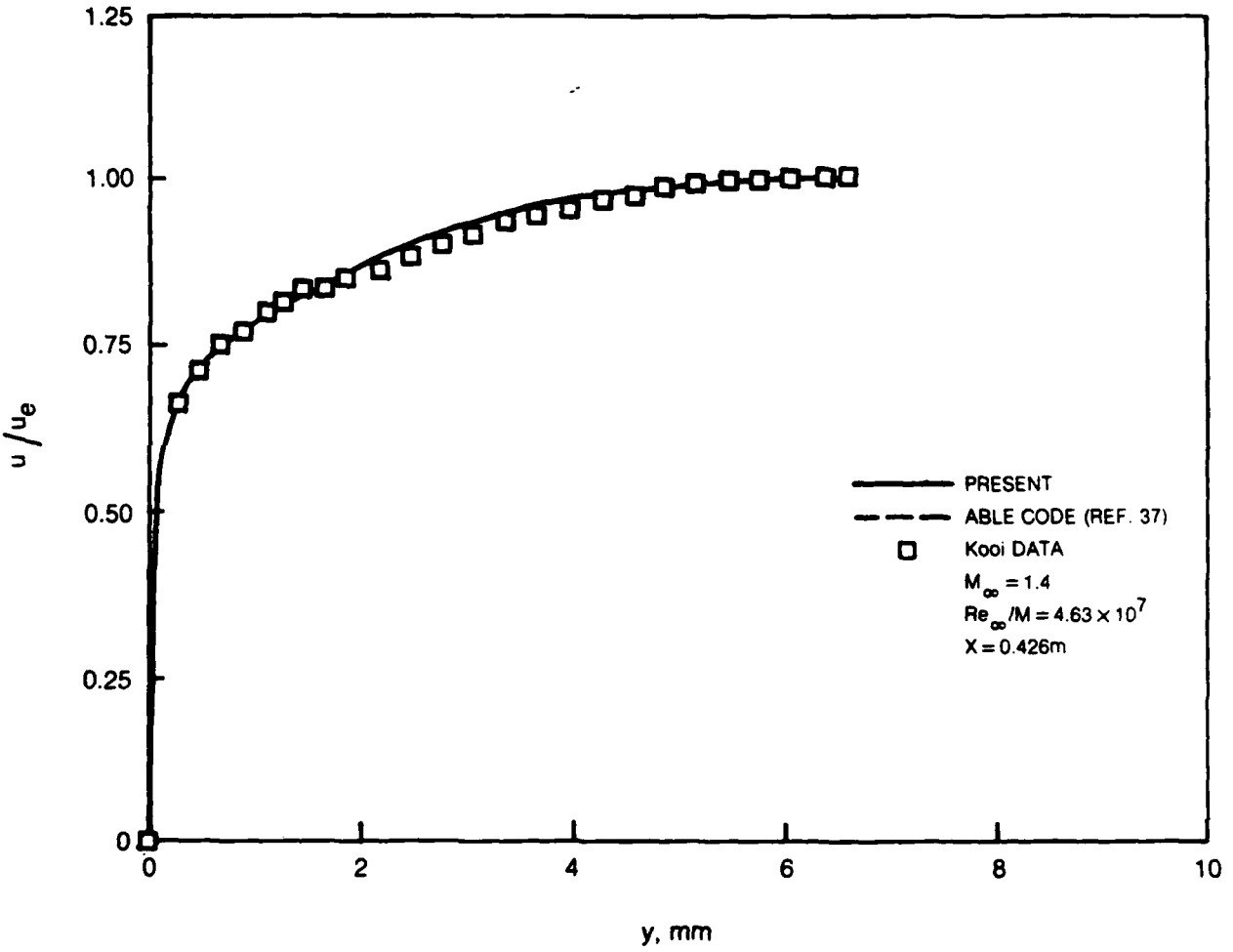

Fig. 17 Comparison of present boundary layer analysis with ABLE code and experimental data c) Undisturbed velocity profile upstream of shock wave

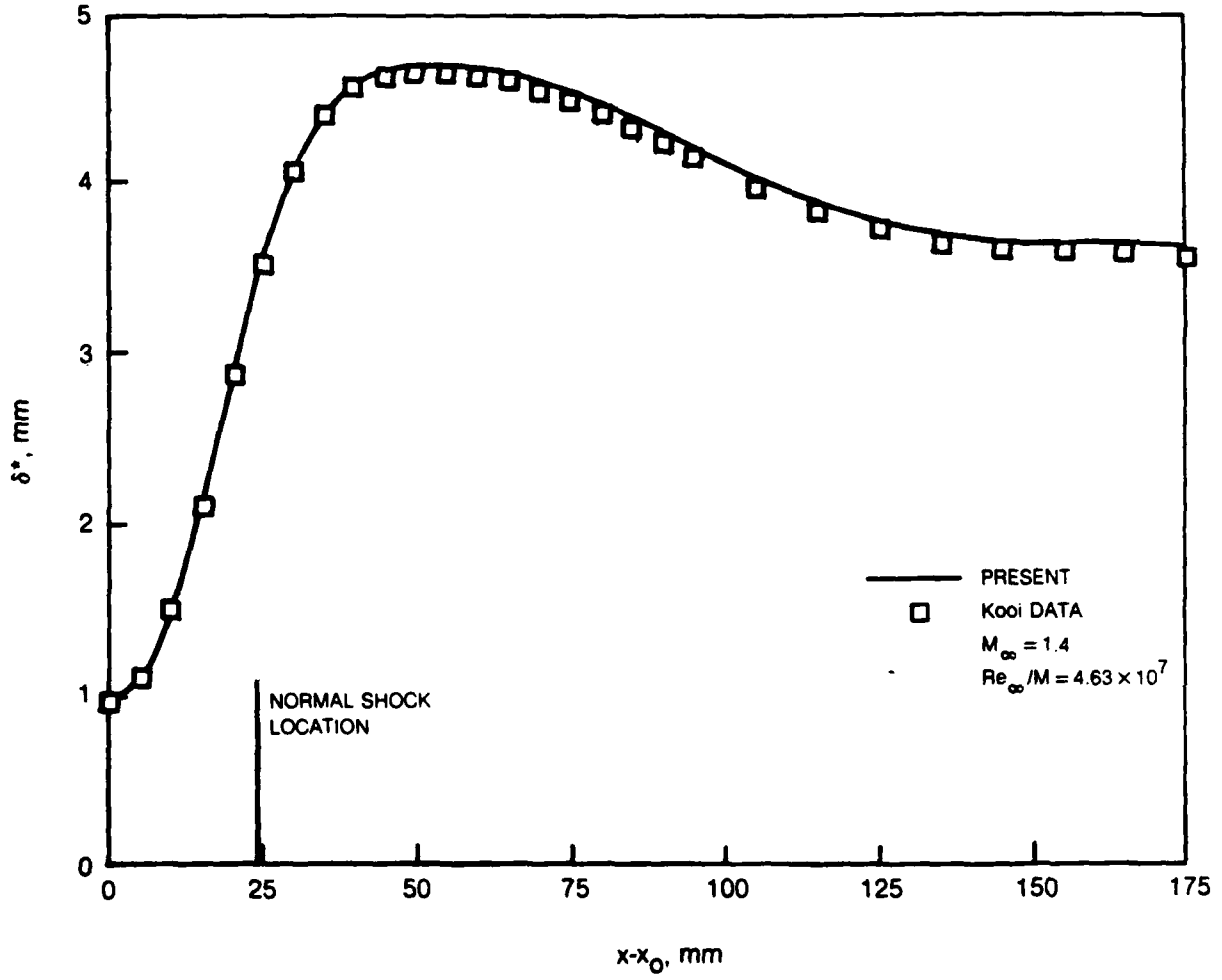

Fig. 18 Inverse boundary layer analysis of transonic normal shock boundary-layer interaction
a) Displacement thickness

82-9-46-5

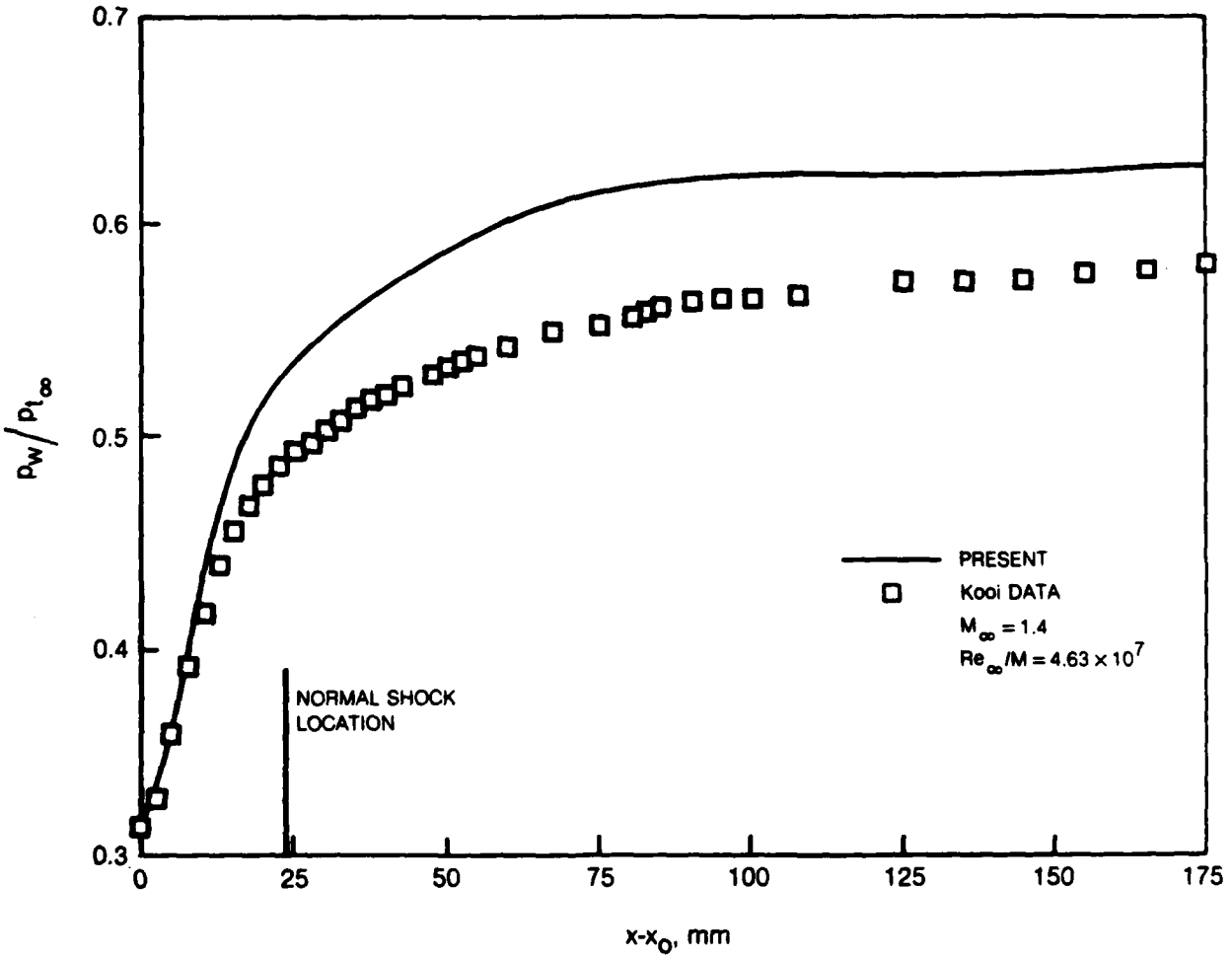

Fig. 18 Inverse boundary layer analysis of transonic normal shock boundary layer interaction b) Wall pressure

82-9-46-6

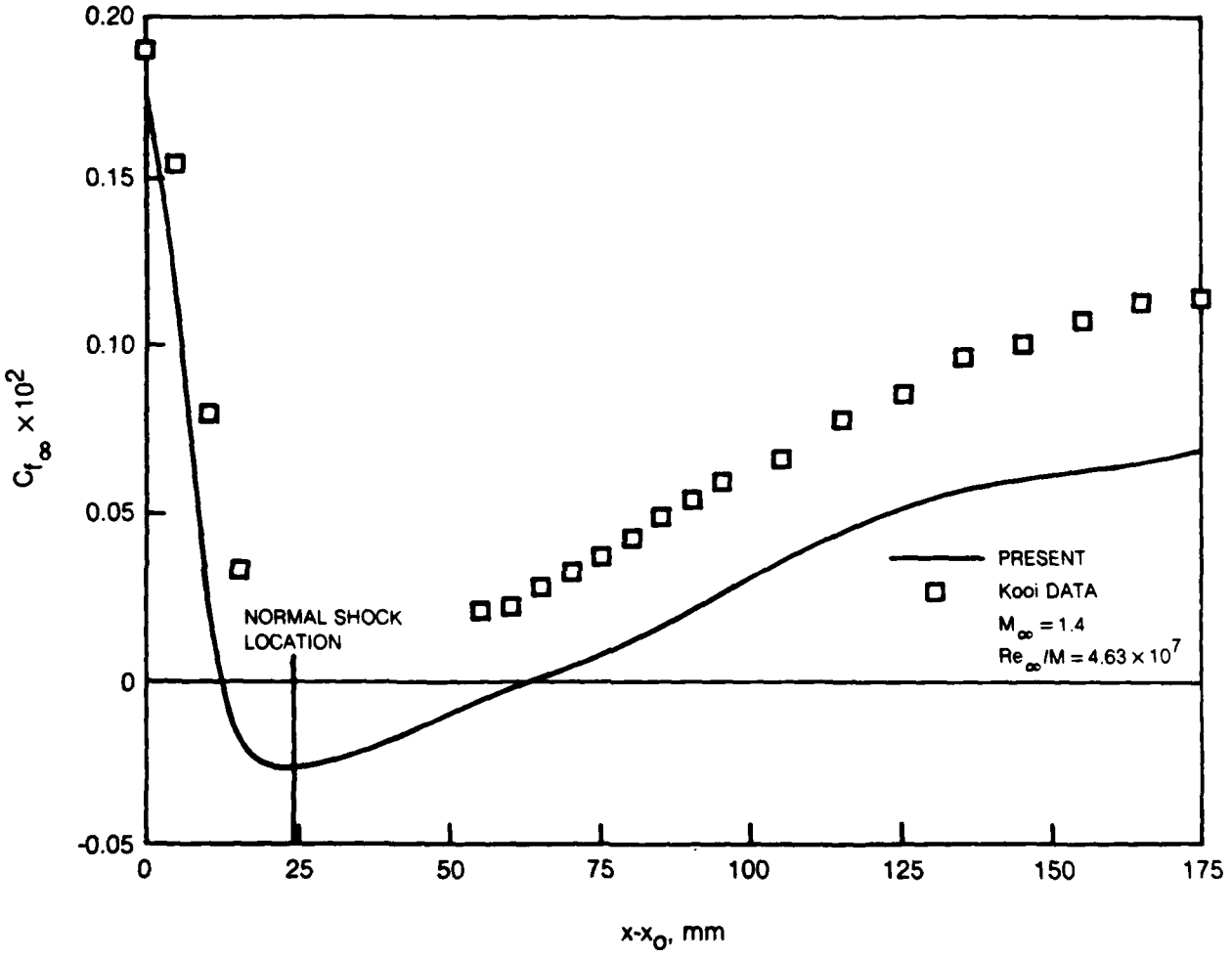

Fig. 18 Inverse boundary layer analysis of transonic normal shock boundary layer interaction c) Skin friction

82-9-46-7

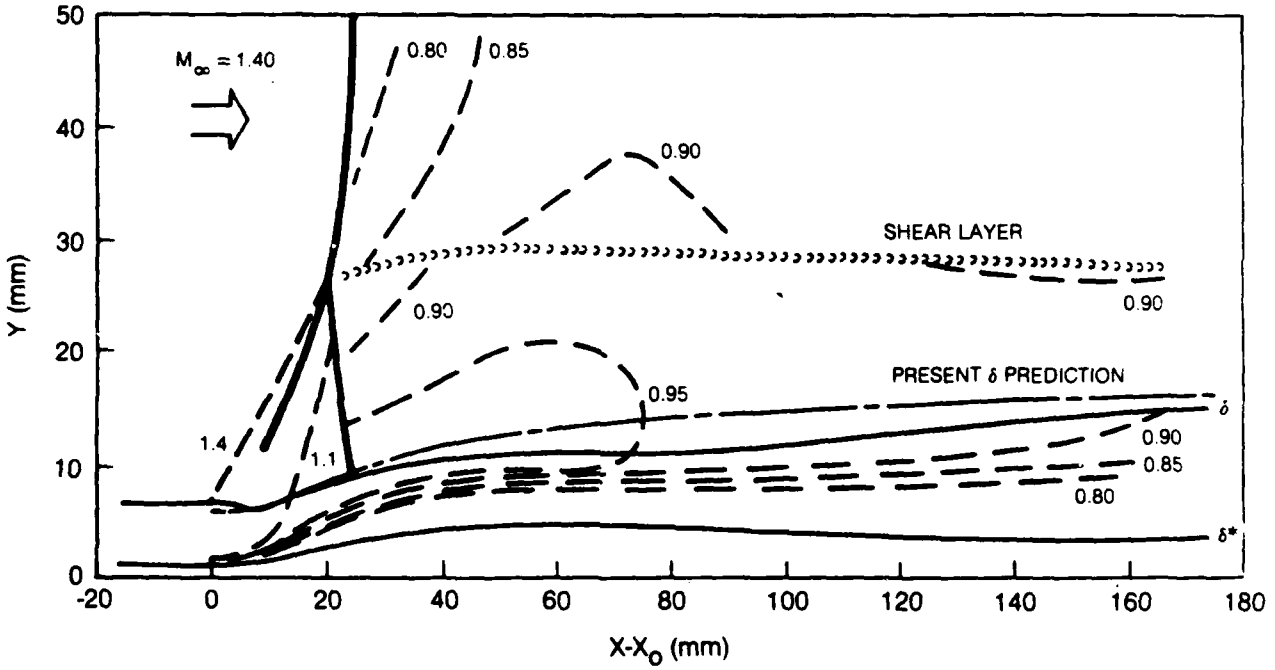

Fig. 19 Comparison of present prediction for boundary layer thickness with Kooi experimental result

APPENDIX A

ANALYSIS OF SEPARATED BOUNDARY-LAYER FLOWS

J. E. Carter and V. N. Vatsa

United Technologies Research Center

East Hartford, CT 06108

Presented at the

Eighth International Conference on

Numerical Methods in Fluid Dynamics

Aachen, West Germany

June 28 - July 2, 1982

ANALYSIS OF SEPARATED BOUNDARY-LAYER FLOWS

J. E. Carter and V. N. Vatsa
United Technologies Research Center
East Hartford, CT 06108/USA

INTRODUCTION

The development of computational procedures for the analysis of separated boundary-layer flows continues to be an active research area since flow separation plays an important role in determining the upper limit of performance of aerodynamic configurations in both external and internal flow. The objective of this paper is to present an overview of a method for predicting the strong interaction between the viscous and inviscid flows which occurs when flow separation exists. In the first part of this paper, a new inverse boundary-layer procedure is briefly presented which approximately accounts for normal pressure gradients that can be important in strongly interacting flows. The second part of this paper focuses on viscous-inviscid interacting flows where the viscous formulation is first-order since the pressure is assumed constant across the boundary layer. Results obtained with this procedure for three separated flow problems are presented: 1) transitional separation bubbles near airfoil leading edges, 2) subsonic boattail separated turbulent flow, and 3) transonic turbulent shock wave boundary-layer interaction on an axisymmetric bump configuration. Comparisons with experimental data and solutions of the Navier-Stokes equations, where available, are also shown.

VISCOUS ANALYSIS INCLUDING NORMAL PRESSURE GRADIENTS

Although the occurrence of flow separation does not lead in all cases to significant normal pressure gradients in the viscous region, there are strongly interacting flows in which this effect can be important. For example, it has been observed experimentally that significant normal pressure gradients are induced in the viscous region when a transonic normal shock wave, of sufficient strength to result in flow separation, impinges on an incoming flat plate turbulent boundary layer. As a first step toward the inclusion of normal pressure gradients in a viscous-inviscid interaction analysis, a generalization of the previous inverse boundary-layer formulation developed by Carter[1] is presented in which the pressure $p(x,y)$ is set equal to the inviscid pressure $p_i(x,y)$, which is deduced from the inviscid flow over the generalized displacement thickness given by

$$\int_0^{\infty} \rho u \, dy = \int_{\delta^*}^{\infty} \rho_i u_i \, dy \tag{1}$$

where the i-subscripted variables denote inviscid flow quantities. In this interaction model, which is similar to that proposed by LeBalleur[2], the inviscid flow is permitted to vary over the scale of the boundary layer in contrast with the usual first order assumption of constant pressure, $p(x,y) = p_i(x,\delta^*)$, where $p_i(x,\delta^*)$ is the inviscid pressure at the displacement thickness.

In order to facilitate the finite-difference solution of this new formulation, the x-momentum, continuity and energy equations are transformed with a modified form of the Levy-Lees transformation given by:

$$\xi = \int_0^x \rho_{\delta^*} u_{\delta^*} \mu_{\delta^*} \left(\frac{r}{r_0}\right)^{2j} dx \qquad \eta = \frac{y}{\delta^*} \tag{2}$$

where x and y are the coordinates along and normal to the surface, respectively,

and the δ^*- subscripted variables denote inviscid quantities on the displacement body. Based on previous work for separated boundary layers, the governing equations and boundary conditions are cast into an inverse formulation in which the pressure on the displacement body is deduced from the solution of the viscous equations for a prescribed streamwise distribution of boundary-layer perturbation mass flow, $m = \rho_{\delta^*} u_{\delta^*} r_o^j \delta^*$. The key to this inverse formulation is the introduction of a perturbation stream function, $\tilde{f}$, which is related to the usual stream function ψ by:

$$\psi = m(\eta - \tilde{f}) + \psi_\Delta \tag{3}$$

where ψ_Δ is the deviation of the inviscid stream function ψ_i from the usual first-order linear variation and is given by $\psi_\Delta = \psi_i - m(\eta - 1)$. With this formulation the surface boundary condition, $\psi = 0$ becomes $\tilde{f} = 0$ since $\psi_\Delta = 0$ at the wall; the outer boundary condition, $\psi \to \psi_i$ as $\eta \to \infty$, becomes $\tilde{f} \to 1$. The use of the stream function automatically guarantees that Eq. (1) is satisfied.

The transformed boundary-layer equations are written as follows in which the pressure gradient $\partial p/\partial x$ has been set equal to the inviscid pressure gradient expressed in the present boundary-layer variables:

$$\frac{\partial \tilde{f}}{\partial \eta} = 1 - \bar{\rho} F + \frac{1}{m} \frac{\partial \psi_\Delta}{\partial \eta} \tag{4}$$

$$m^2 \beta F \frac{\partial F}{\partial \xi} - m \frac{\partial}{\partial \xi}\left[m(\eta - \tilde{f}) + \psi_\Delta\right] \frac{\partial F}{\partial \eta} = m^2 \beta (\bar{\rho}_i F_i^2 - \bar{\rho} F^2) + m^2 \bar{\rho}_i F_i \frac{\partial F_i}{\partial \xi} - m \frac{\partial \psi_i}{\partial \xi} \frac{\partial F_i}{\partial \eta} + \frac{\partial}{\partial \eta}\left(\bar{\mu}_1 \frac{\partial F}{\partial \eta}\right) \tag{5}$$

$$m^2 \bar{\rho} F \frac{\partial g}{\partial \xi} - m \frac{\partial}{\partial \xi}\left[m(\eta - \tilde{f}) + \psi_\Delta\right] \frac{\partial g}{\partial \eta} = \frac{1}{Pr} \frac{\partial}{\partial \eta}\left[\bar{\mu}\left(1 + \frac{\epsilon}{\mu} \frac{Pr}{Pr_t}\right) \frac{\partial g}{\partial \eta}\right] + \alpha \frac{\partial}{\partial \eta}\left[\bar{\mu}\left(1 - \frac{1}{Pr}\right) \frac{\partial F^2/2}{\partial \eta}\right] \tag{6}$$

in which the following definitions have been used

$$F = \frac{u}{u_{\delta^*}} \quad \bar{\rho} = \frac{\rho}{\rho_{\delta^*}} \quad g = \frac{H}{H_{\delta^*}} \quad \bar{T} = \frac{T}{T_{\delta^*}} \quad \bar{\mu} = \frac{\mu}{\mu_{\delta^*}} \quad \bar{\mu}_1 = \frac{\epsilon + \mu}{\mu_{\delta^*}} \quad \alpha = \frac{u_{\delta^*}^2}{H_{\delta^*}} \quad \beta = \frac{1}{u_{\delta^*}} \frac{du_{\delta^*}}{d\xi} \tag{7}$$

In these equations ϵ is the eddy viscosity coefficient for turbulent flows for which the algebraic turbulence model of Cebeci-Smith[3] has been used. The laminar and turbulent Prandtl numbers are denoted by Pr and Pr_t, respectively. Equations (4)-(6) are solved with an implicit finite-difference scheme for $\tilde{f}$, F, g and the unknown pressure gradient parameter β for a prescribed m-distribution and with the inviscid flow solution over the generalized displacement body assumed known. The boundary conditions are given by

$$\begin{aligned} &\eta = 0 \quad F = \tilde{f} = 0 \quad g = g_w \\ &\eta \to \infty \quad F \to F_i \quad \tilde{f} \to 1 \quad g \to 1 \end{aligned} \tag{8}$$

The density is deduced from the state equation $\bar{\rho} = (\bar{\rho}_i \bar{T}_i)/\bar{T}$ after the normalized static temperature $\bar{T}$ is deduced from the definition of total enthalpy, H. An important feature of this formulation is that as the boundary-layer edge is approached and the viscous shear and heat conduction terms vanish, the viscous flow solution is required to asymptotically approach the inviscid solution over the generalized

displacement body. Further details of this generalized inverse boundary-layer formulation and computed examples are given by Carter and Hafez.[4]

The computed results presented in this paper were obtained with a first-order viscous formulation which is deduced by setting $\psi_\Delta = 0$ and $\bar{\rho}_1 = F_1 = 1$ in Eqs. (4)-(6). In the actual calculations the first-order inverse boundary-layer formulation presented by Carter[1] was used; however, these two inverse boundary-layer formulations are quite similar and one can easily be derived from the other by a slight change in the definition of the perturbation stream function, transformed normal coordinate, and the pressure gradient parameter.

INTERACTION ITERATION PROCEDURE

The present analysis is based on a global viscous-inviscid iteration technique, previously presented by Carter,[1] in which the inverse boundary-layer solution is solved iteratively with a direct analysis of the inviscid flow including injection to represent the displacement thickness effects. The key feature of this iteration procedure is the simple update formula

$$m^{i+1} = m^i \left[1 + \omega\left(\frac{u_{e_V}}{u_{e_I}} - 1\right)\right] \tag{9}$$

where ω is the relaxation factor, and u_{e_V} and u_{e_I} denote the viscous and inviscid predictions, respectively, of the velocity tangent to the displacement body for the m-distribution at the ith global iteration. This update procedure, which is similar to that used by LeBalleur,[2] is general as it has been used with a variety of inverse boundary-layer and direct inviscid solution procedures as pointed out in Ref. 1.

RESULTS AND DISCUSSION

In this section three applications of the first-order viscous-inviscid interaction analysis are presented. In each case a brief discussion is given of the particular features of each analysis and the inviscid solution procedure which was utilized. References are given for each of these applications in which a more detailed discussion is presented.

Airfoil Leading-Edge Separation Bubbles

The first application of this interaction theory is for the transitional separation bubble which occurs near the leading edge of an airfoil. If the Reynolds number is sufficiently low such that the boundary layer remains laminar up to the point of minimum pressure, then the onset of the adverse pressure gradient generally results in separation of the laminar boundary layer; subsequently, transition from laminar to turbulent flow occurs in the separated shear layer, and if the bubble does not burst, then turbulent reattachment occurs further downstream. Since the streamwise length scale of this viscous-inviscid interaction is typically only a few percent of the airfoil chord, this localized interaction is treated as a perturbation to a global viscous airfoil analysis, which in the present effort was the GRUMFOIL code developed by Melnik, et. al[5]. The deviation of the edge velocity, u_e, due to the transitional bubble, from the reference global airfoil solution is represented by a Cauchy integral given by

$$u_{e_I} = u_{e_{ref}} + \frac{1}{\pi}\int_{s_1}^{s_2} \frac{\frac{d}{d\xi}\left[u_e\left(\delta^* - \delta^*_{ref}\right)\right] d\xi}{s - \xi} \tag{10}$$

in which the source strength is proportional to the streamwise derivative of the corresponding deviation in the displacement thickness.

The local interaction analysis was applied to the transitional separation bubble, measured experimentally by Gault[6], which occurs at the leading edge of a NACA 66_3-018 airfoil at a chord Reynolds number of 1.5×10^6 and $\alpha = 12$ deg. At this angle of attack, the reference solution, obtained from the GRUMFOIL code, was found to significantly overpredict the lift coefficient for this airfoil. Correspondingly the pressure in the strong acceleration region was overpredicted thereby providing an inaccurate reference solution for this case. These errors are probably due to the inability of the GRUMFOIL code to correctly model the lift decrement due to the massive trailing edge separation which occurred in this case at 0.75 chord on the upper surface. In order to compensate for this problem, the GRUMFOIL code was run at a reduced angle of attack at 11.25° which provided a much better match of the experimental lift coefficient and the pressure distribution between the stagnation point and the peak suction region as shown in Fig. 1(a).

The transition model used in the present calculation is the streamwise intermittency function of Dhawan and Narasimha[7] which requires the specification of the onset and length of the transition region. In the present case the onset of transition was assumed to occur midway between the experimental separation point and the "break" point in the experimental pressure distribution shown in Fig. 1. The length of the transition region was established so that the intermittency function had a value of $\gamma = 0.5$ at the experimental pressure "break" point.

The computed results for this case are shown in Figs. 1(a) and 1(b) for the pressure, and skin friction and displacement thickness, respectively. The good agreement shown between the predicted results and Gault's pressure data and measured separation point verifies the use of a local interaction model for the airfoil leading edge transitional bubble problem. Figure 1(a) also shows the inviscid airfoil pressure distribution which was obtained from the GRUMFOIL code with $\alpha = 11.25°$. The large difference between this solution and the viscous airfoil solution obtained with the GRUMFOIL code shows the importance of including the viscous effects in the reference solution which is input to the present perturbation interaction analysis. Further details of this interaction analysis and other computed examples are presented by Carter and Vatsa.[8]

Subsonic Boattail Separated Turbulent Flow

The second application presented in this paper is the subsonic turbulent separated flow in the juncture region of an axisymmetric boattail-sting configuration. The conservative full potential analysis of Green[9] was used to represent the outer inviscid flow. In order to reduce the injection velocity associated with the large displacement thickness growth which occurs in the boattail-sting juncture region, the inviscid flow was solved over a shear layer coordinate which was assumed a priori to approximate the displacement body position. Injection was then used along this shear layer coordinate, but the injection magnitude was significantly reduced since it was now proportional only to the difference between the assumed and the actual displacement body locations. The boundary-layer equations are also expressed in terms of this shear layer oriented coordinate system, but the usual form of these equations is recovered with the use of the Prandtl transposition theorem.

Figure 2 shows the computed pressure and skin friction distributions from both the present interaction analysis and the numerical solution of the Navier-Stokes equations[10] for the $M_\infty = 0.7$ flow over the circular-arc boattail-sting configuration measured experimentally by Reubush.[11] Figure 2 shows excellent agreement between the two theoretical analyses, thereby confirming that the neglected terms in the approximate interaction analysis are of secondary importance in this separated flow

case. Nonetheless it is observed that both analyses overpredict the experimental pressure in the separated region and predict the separation point too far downstream. This discrepancy was thought to be due to the use of the Cebeci-Smith algebraic turbulence model as it has been observed in other analyses of separated flow to result in an underprediction of the displacement thickness and a corresponding overprediction of the pressure in regions of strong adverse pressure gradient. This observation led Shang and Hankey[12] to modify the algebraic turbulence model through a global streamwise relaxation model which approximately accounts for the so-called "history of the flow." Figure 3 shows the computed results which were obtained with the Shang-Hankey model implemented into both the interaction and the Navier-Stokes analyses. The overall agreement with the experimental data is significantly improved with the use of this model, although it is observed that the interacting boundary-layer results show greater sensitivity to this modification than the Navier-Stokes analysis thereby giving better agreement with the experimental data.

Transonic Shock Wave Boundary Layer Interaction

The third application of this viscous-inviscid interaction approach is the transonic shock induced separated flow over an axisymmetric circular arc-bump configuration for which experimental data and a solution of the Navier-Stokes equations were given by Johnson, et. al.[13] Calculations using the present approach for this configuration have previously been presented by Carter;[1] however, several numerical improvements have been made in the interim and these are briefly discussed here with more details given in Ref. 14.

In the previous calculations it was found necessary to use numerical smoothing to eliminate oscillations which occurred when the fully conservative potential analysis of Green[9] was used with the inverse boundary-layer analysis. It was found in the present work that these oscillations were eliminated, and hence the need for smoothing, by placing a grid point on the shear layer coordinate to precisely correspond to the location of the body-sting corner, and by using central differencing of the displacement thickness in the inviscid transformed plane to numerically compute the injection velocity. In addition, it was found that using the same x-grid in both the viscous and inviscid calculations, which eliminates interpolation between the two solutions, enhanced the overall interaction convergence rate. Figure 4 shows the computed pressure and displacement thickness distributions in comparison with the experimental data and Navier-Stokes calculation presented by Johnson, et. al.[13] The interaction calculations were made with both the nonconservative potential flow analysis of South[15] and the conservative analysis of Green.[9] In contrast with the Navier-Stokes solution both analyses show good agreement with the data for the shock wave position. It is well known that in an inviscid analysis a conservative potential flow calculation predicts a stronger shock wave located downstream of that given by a nonconservative computation. The present results show that this difference is significantly reduced when viscous interaction effects are included since the stronger shock given by the conservative analysis produces a larger displacement thickness, as shown in Fig. 4(b), thereby weakening the shock and moving it forward to place it in better agreement with that predicted by the nonconservative analysis.

As was found in the subsonic boattail calculation, this interaction calculation overpredicts the pressure and underpredicts the displacement thickness in comparison with the data in the body-sting juncture region. This difference is probably due to the algebraic turbulence model and can be substantially reduced by use of the Shang-Hankey[12] model or by reducing the Clauser constant, as was shown by Carter[1], in the outer region eddy viscosity model.

CONCLUDING REMARKS

The applicability of the viscous-inviscid interaction analysis presented herein to various separated flow problems has been demonstrated. Overall, good agreement with experimental data has been observed with this analysis, although it is concluded from these calculations that the use of an algebric turbulence model is inadequate for flows with significant turbulent separated flow. In addition, the generalization of the first-order inverse boundary-layer analysis to approximately account for normal pressure gradients has been presented. It now remains to combine this new viscous analysis with an inviscid solution procedure and demonstrate its use in viscous-inviscid interacting flows.

ACKNOWLEDGEMENTS

The authors express their graditude for the support of this work to the following technical monitors and agencies: James D. Wilson, Air Force Office of Scientific Research; Joel L. Everhart, NASA-Langley Research Center; and Robert E. Whitehead, Office of Naval Research.

REFERENCES

1. Carter, J. E.: AIAA Paper No. 81-1241, 1981.
2. Leballeur, J. C.: La Recherche Aerospatiale, English Edition, pp. 21-45, 1981-3.
3. Cebeci, T. and A. M. O. Smith: *Analysis of Turbulent Boundary Layers*, Academic Press, 1974.
4. Carter, J. E. and M. Hafez: AFOSR Report to be published, 1982.
5. Melnik, R. D., R. Chow, and H. R. Mead: AIAA Paper No. 77-680, 1977.
6. Gault, D. E.: NASA TN 3505, 1955.
7. Dhawan, S. and R. Narasimha: J. Fluid Mechanics, Vol. 3, 1958.
8. Carter, J. E. and V. N. Vatsa: NASA CR-165935, 1982.
9. Green, L. L.: AIAA Paper No. 81-1204, 1981.
10. Vatsa, V. N., J. E. Carter, and R. D. Swanson: ISCME Conference, Washington, D. C., June 30-July 2, 1982.
11. Reubush, D. E.: NASA TN D-7795, 1974.
12. Shang, J. S. and W. L. Hankey, Jr.: AIAA Journal, Vol. 13, pp. 1368-1374, 1975.
13. Johnson, D. A., C. C. Horstmann, and W. D. Bachalo: AIAA Journal, Vol. 20, No. 6, pp. 737-744, 1982.
14. Carter, J. E. and V. N. Vatsa: ONR Report to be published, 1982.
15. South, J. C. and A. Jameson: AIAA CFD Conference, 1973.

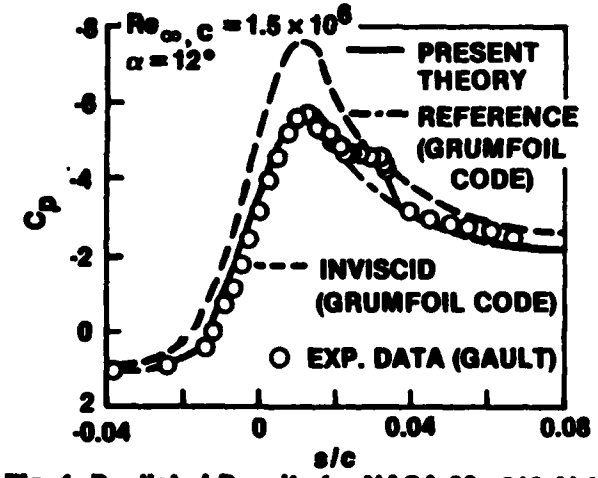

Fig. 1 Predicted Results for NACA 66_3-018 Airfoil
a) Pressure

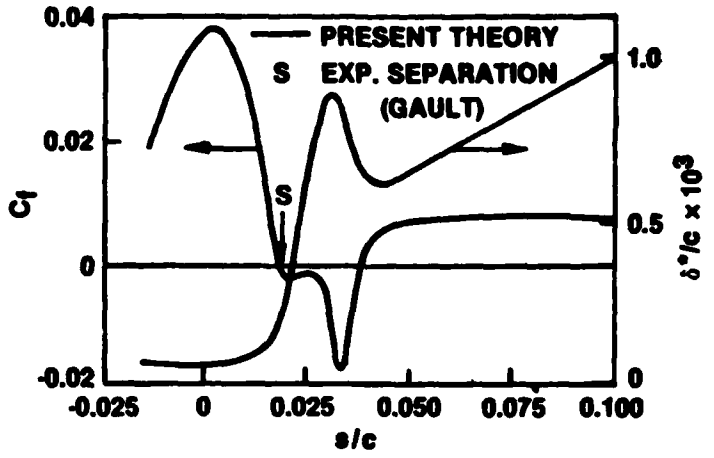

Fig. 1(b) Skin Friction and Displacement Thickness

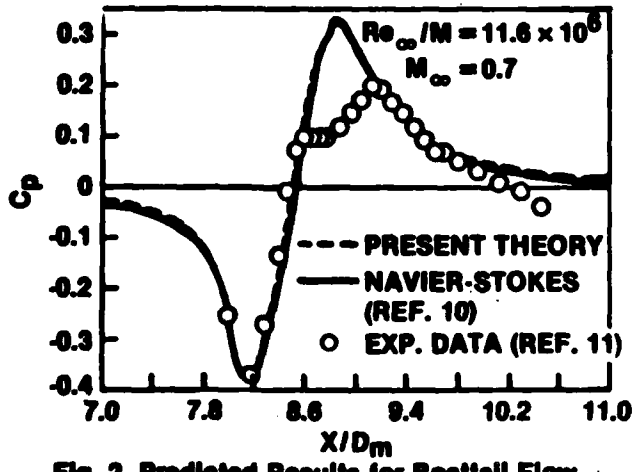

Fig. 2 Predicted Results for Boattail Flow
a) Pressure

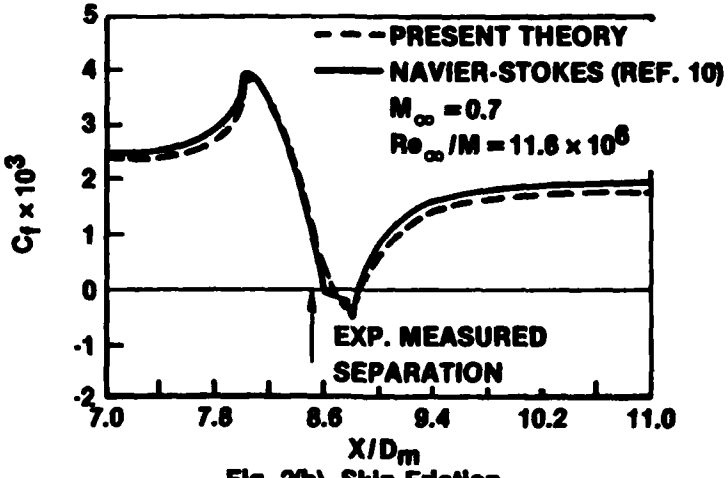

Fig. 2(b) Skin Friction

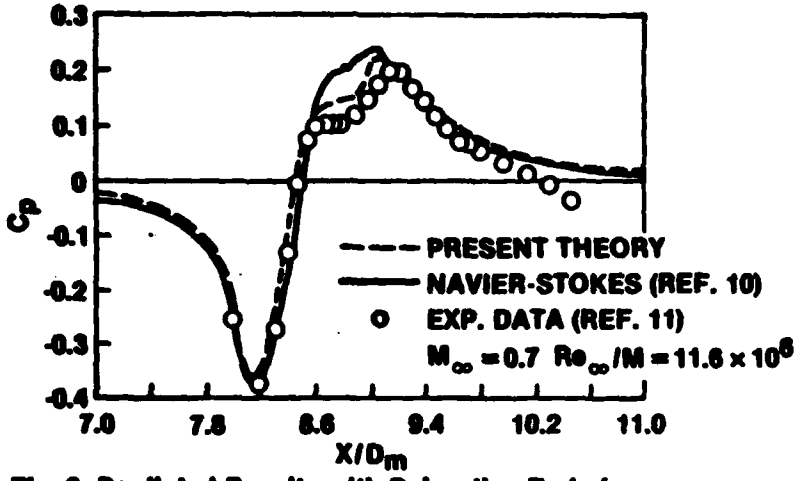

Fig. 3 Predicted Results with Relaxation Turbulence Model for Boattail Flow. a) Pressure

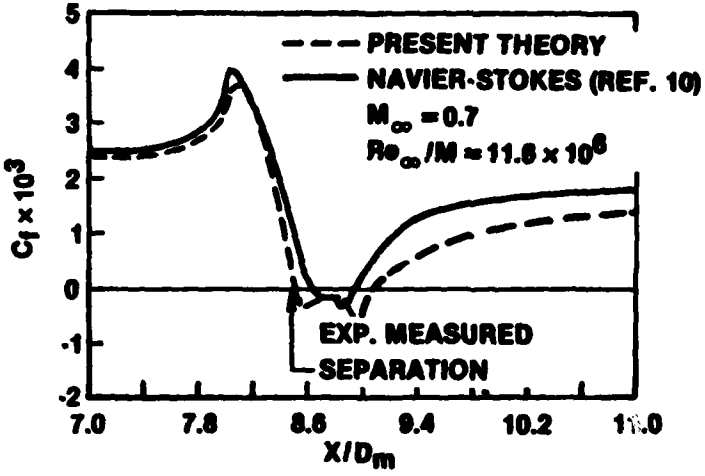

Fig. 3(b) Skin Friction

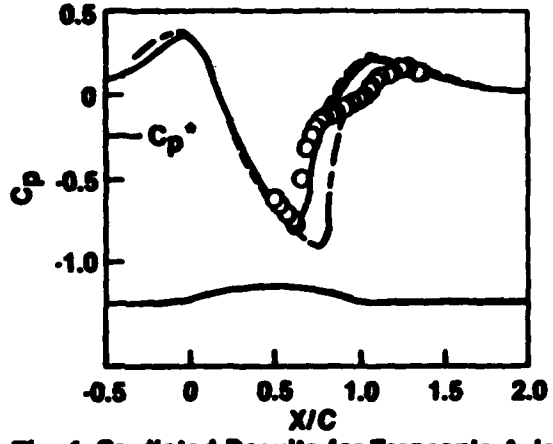

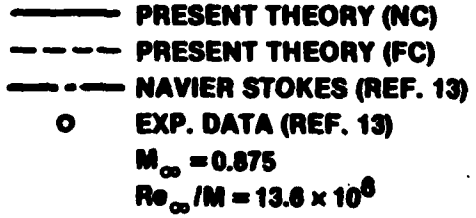

Fig. 4 Predicted Results for Transonic Axisymmetric Flow (a) Pressure

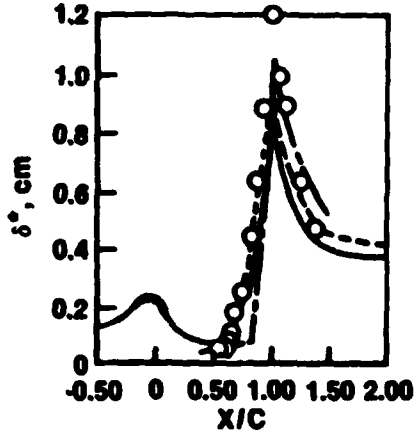

Fig. 4(b) Displacement Thickness

END

FILMED